Journal of Energy Storage 174 (2026) 123129

Contents lists available at ScienceDirect

Journal of Energy Storage

journal homepage: www.elsevier.com/locate/est

Research Papers

Proper battery modelling to schedule an isolated microgrid with a chance constrained spinning reserve☆

Matteo Spiller[a,*], Riccardo Nebuloni[a], Marco Merlo[a]

[a] Politecnico di Milano, Energy Department, Piazza Leonardo da Vinci 32, 20133, Milano, Italy

ARTICLE INFO

Keywords:
BESS
Round-trip efficiency
Capacity fade
Chance-constrained
Isolated Microgrid

ABSTRACT

Accurate modelling of battery energy storage systems (BESS) plays a crucial role in the optimal scheduling and planning of isolated microgrids with high penetration of renewable energy sources (RES). However, most mixed-integer linear programming (MILP) based scheduling models neglect the simultaneous representation of efficiency and degradation effects, which leads to inaccurate cost estimation and suboptimal operational decisions. This paper proposes an advanced MILP formulation for isolated microgrid scheduling that integrates a linearised BESS model capturing variable efficiency and combined cycle and calendar ageing to represent the capacity fade of the asset. The two ageing models integrated into the MILP formulation are data-driven, built upon publicly available open-access datasets. The formulation linearises efficiency and calendar ageing characteristics through a piecewise affine interpolation approach, which achieves high modelling accuracy while maintaining computational tractability.

The study validates the BESS model through two distinct formulations applied to a real-world isolated microgrid case study supplying Lipari Island in Italy. A deterministic planning simulation demonstrates the model's low computational effort. The proposed BESS formulation uses only two binary variables per time step and optimises a full-year horizon (8760 time steps) in less than 20 s. The results show that explicitly modelling efficiency variations and battery degradation strongly affects scheduling decisions and operating costs. In addition, the paper evaluates the performance of the BESS model proposed in a 24-hour chance-constrained spinning reserve formulation that ensures reliable microgrid operation under uncertainty. The BESS model integrates seamlessly with this complex formulation and confirms that the storage deployment improves microgrid reliability without increasing operating costs.

Set	Description
t	Time instants
g	Generators
k	Piecewise affine interpolation losses breakpoints
s	Piecewise affine interpolation losses segments
a	Piecewise affine interpolation ageing segments
w	Chance-constrained discrete probability density function intervals

Parameter	Description	Unit
π^{diesel}	Diesel cost per kWh	€/kWh
π^{start}	Diesel generator start-up cost	€
π^{cost}	Energy lost cost	€/kWh
$P_t^{PV\ kW}$	PV power in kW	kWh
P_t^{load}	Load electrical power	kWh
P_{min}^{diesel}	Diesel minimum power	kW
P_{max}^{diesel}	Diesel maximum power	kW
P_k^{BESS}	BESS power breakpoints	Per unit
$efficiency_k$	Efficiency breakpoints	Per unit
$losses_k$	Losses breakpoints	Per unit
M_s^{losses}	Losses angular coefficient	Per unit
Q_s^{losses}	Losses intercept	Per unit
P_{nom}^{BESS}	BESS nominal power	kW
E_{nom}^{BESS}	BESS nominal energy	kWh
B	Cycle ageing coefficient	Per unit
M_a^{ageing}	Ageing angular coefficient	Per unit
Q_a^{losses}	Ageing intercept	Per unit
SoC_a	SoC breakpoints	Per unit
$Time_t^{ageing}$	Calendar ageing time dependency	Hours

(continued on next column)

(continued)

(continued on next page)

☆ This article is part of a Special issue entitled: 'ICSET 2025-Energy Storage' published in Journal of Energy Storage.

* Corresponding author.
E-mail address: matteo.spiller@polimi.it (M. Spiller).

https://doi.org/10.1016/j.est.2026.123129
Received 30 December 2025; Received in revised form 14 May 2026; Accepted 10 June 2026
Available online 18 June 2026

(*continued*)

T_0	BESS calendar life	Hours
$P_{t,w}$	Reserve demand	kW
α	Confidence level	–
$E_{t,w}^{res\ up}$	Discrete upward reserve demand	kW
$E_{t,w}^{res\ down}$	Discrete downward reserve demand	kW
τ	Big number	

Variable	Description	Unit
$p_{t,g}^{diesel}$	Diesel energy	kWh
$x_{t,g}^{start}$	Diesel start up binary	Per Unit
e_t^{lost}	Energy lost	kWh
$p_t^{dis\ ac\ kW}$	BESS AC discharge power	kWh
$P_t^{cha\ ac\ kW}$	BESS AC charge power	kWh
$x_{t,g}^{diesel}$	Diesel status	Per unit
$Losses_t^{cha}$	BESS charge losses	Per unit
$Losses_t^{dis}$	BESS discharge losses	Per unit
$p_t^{cha\ ac}$	BESS AC charge power in per unit	Per unit
$p_t^{dis\ ac}$	BESS AC discharge power in per unit	Per unit
$p_t^{cha\ dc}$	BESS DC charge power in per unit	Per unit
$p_t^{dis\ dc}$	BESS discharge power in per unit	Per unit
z_t^{cha}	BESS binary for charging	Per unit
z_t^{dis}	BESS binary for discharging	Per unit
SoC_t	BESS state of charge	Per unit
E_{nom}^{BESS}	BESS energy content	kWh
$C_{fade}^{calendar}t$	Capacity fade due to calendar ageing	Per unit
$A(SoC)_t$	Calendar ageing contribution as function of the SoC	Per unit
$C_{fade}^{cycle}t$	Capacity fade due to cycle ageing	Per unit
SoH_t	BESS state of health	Per unit
SR_t	Microgrid spinning reserve	kW
L_t	Microgrid residual load	kW
$SR_{t,g}^{up\ diesel}$	Diesel generator upward spinning reserve	kW
$SR_{t,g}^{down\ diesel}$	Diesel generator downward spinning reserve	kW
$SR_t^{up\ BESS}$	BESS upward spinning reserve	kW
$SR_t^{down\ BESS}$	BESS downward spinning reserve	kW
SR_t^{up}	Upward spinning reserve	kW
SR_t^{down}	Downward spinning reserve	kW
$W_{t,w}$	If-else condition binary variable	–
SR_t^{down}	Microgrid downward spinning reserve	kW
SR_t^{up}	Microgrid upward spinning reserve	kW

1. Introduction

The current decarbonisation targets set by the EU drive the integration of renewable energy sources (RES), such as wind and photovoltaic (PV), in the energy sector [1]. Despite the limited carbon footprint of RES, their inherent limited inertia and production unpredictability pose significant challenges to the planning and operation of the electric power system. Although the complete decarbonisation of the EU energy sector is forecasted by 2050, the development of tools to correctly integrate RES is essential to smoothly achieve the decarbonisation target. In this perspective, isolated microgrids, due to their inherent limited amount of resources, are the systems that in the coming future will face major problems with RES [2].

Lithium-ion large-scale battery energy storage system (BESS) plays a crucial role in coping with frequency oscillations and production uncertainty related to RES. According to the International Energy Agency (IEA) [3], the widespread adoption of BESS drastically reduced the capital expenditures of this asset. Nevertheless, the limited amount of energy and the degradation that affects their performances throughout their operating life call for tools capable of accurately characterising the performances and the degradation of BESS, and effectively managing the energy storage are now more than ever vital for the energy transition.

To ensure an efficient operation of the asset, approaches such as rule-based methods and model predictive control (MPC) have been proposed in the literature to schedule BESS in several applications. However, mixed integer linear programming (MILP) offers significant advantages in defining BESS optimal schedules, particularly in its ability to handle complex operational constraints and to account for uncertain input parameters [4].

Generally, the goal of effective scheduling in isolated microgrids is to define the optimal day-ahead scheduling of the microgrid resources to balance consumption and generation at every time instant. This means that the load must always be equal to the energy produced by traditional generators and RES. BESS in isolated microgrids are crucial to address the uncertainty, ensuring the operation reliability and the security of supply. Deterministic MILP formulations have been widely adopted for the optimal scheduling of isolated microgrids integrating RES, conventional generators, and BESS [5]. However, increasing RES penetration introduces significant uncertainty in generation adequacy, requiring appropriate spinning reserve allocation to avoid involuntary load shedding [6]. Traditional reserve estimation methods rely on deterministic rules based on the largest online unit or a fraction of the load demand [7] but these approaches neglect the stochastic nature of RES and load variability. Consequently, probabilistic and chance-constrained formulations have been proposed to improve reserve allocation and balance operational reliability against economic performance [8,9]. Authors in [10] are the first to address the spinning reserve problem in a microgrid. They adopt a probabilistic load, wind and PV model and formulated an MILP problem to provide the spinning reserve to a microgrid in case of different orders of outages. [11] improved the probabilistic formulation by modelling the uncertainty of the spinning reserve with a chance-constrained programming, proving the adequacy of the approach in identifying a trade-off between risk awareness and efficient management of the system.

Although chance-constrained formulations improve reserve allocation under RES uncertainty, existing studies generally rely on simple BESS representations based on constant efficiency and neglect battery degradation effects. Nevertheless, as stated in [12], BESS efficiency includes the performance of the cells, power conversion system (PCS) and transformer. The accurate representation of this non-linear performance within a MILP framework requires appropriate linearization techniques. In [13] authors propose a laboratory procedure to characterise the dependence between cell charging capability and SOC. Using experimental results, the authors accurately represent BESS efficiency by accounting for the reduced charging capacity that occurs when the battery transitions from constant-current to constant-voltage charging. This approach is particularly relevant for high C-rate applications, such as EVs. However, implementing such capability curves in optimisation models introduces a significant computational burden and does not accurately reflect the behaviour of large-scale BESS, whose capability curves are typically rectangular in modern applications [14]. [12] models the performances of a BESS with a dynamic stair-wise efficiency function of power within a MILP framework. However, the adopted efficiency model considers the cell performances and does not account for the impact of the PCS and transformer on the overall efficiency. In [15], the authors present three different BESS models by scaling the performance of a single Sanyo 2.05 Ah NMC cell to represent a 10 MWh BESS. They modelled the losses as a function of both the exchanged power and the SOC with a piece-wise linear function, demonstrating that assuming constant efficiency can lead to an overestimation of up to 10% in applications related to energy arbitrage. Nevertheless, this piecewise approach increases computational effort by a factor that spans from 30% to 100% for a daily optimisation compared to the constant-efficiency model, imposing significant limitations for its use in planning and operations problems under uncertainty. In [16], a similar analysis is presented using an efficiency curve derived from an experimental campaign on an NMC BESS. The study proposes three different approaches to interpolate the efficiency curve. The simplest, referred to as “fast-piecewise,” demonstrates high accuracy and low computational effort, making it suitable for real-time applications. However, its formulation may be limited when applied to different performance maps or to MILP formulations different from the tested case study. Authors in [17] adopt the efficiency curve coming from the same experimental campaign, but the MILP algorithm employs a discretised approximation approach to

Table 1
Literature review summary.

Reference	BESS efficiency	Ageing	Ageing data source	Ageing stress factor	Online ageing	Application	Uncertainty
[7]	None	None	None	None	None	Spinning reserve requirements	Iterative probabilistic approach
[10]	Constant	None	None	None	None	Microgrid scheduling	Probabilistic spinning reserve
[11]	Constant	None	None	None	None	Microgrid scheduling	Chance-constrained spinning reserve
[32]	Constant	None	None	None	None	Microgrid scheduling	Robust
[13]	Constant	None	None	None	None	Energy arbitrage	None
[12]	Stair-wise efficiency as a function of BESS power	None	None	None	None	Peak shaving	None
[33]	Efficiency as a function of SOC and power	None	None	None	None	Energy arbitrage	None
[16]	Efficiency as a function of SOC and power	None	None	None	None	MV microgrid	None
[17]	Interpolated as a function of the power	Cycle and calendar	[34] not publicly available	DoD (cycle), temperature (calendar)	None	Energy arbitrage	None
[20]	Constant	Cycle	Not specified	DOD	None	Energy arbitrage and ancillary services	None
[30]	Constant	Calendar and cycle	Derived from [35,36] whose data are not publicly available,	SOC (calendar) Ah (cycle)	None	V2G	None
[26]	Linear efficiency	Cycle	Variable lifecycle	Ah	Yes	Microgrid	None
[27]	Constant	Cycle	Fixed lifecycle	Ah, DoD	No	EV	None
[21]	Constant	Cycle	Derived from [37]	SOC DOD	None	Energy arbitrage and ancillary services	None
[31]	Constant	Cycle+calendar		DoD (cycle), SoC (calendar)	None		
This work	Variable	Cycle+calendar	Open Access Database	FEC (cycle) + SoC (calendar)	Yes	Isolated microgrid	Chance-constrained spinning reserve

solve an arbitrage problem. In [15] a hierarchical two-level MILP applies a piecewise affine interpolation technique to linearise the efficiency of lithium-ion cells. While this method provides a robust and computationally efficient formulation, it is applied only at the cell level and does not extend the approach to a complete BESS efficiency modelling.

Existing MILP formulations demonstrated that variable-efficiency BESS models improve scheduling accuracy. However, these approaches significantly increase computational complexity and have only been validated in deterministic optimisation problems. Moreover, no study has evaluated model performance under uncertainty or incorporated lithium-ion cell ageing using publicly available datasets. The latter aspect is vital for the planning and operation of BESS. Indeed, the inclusion of the degradation in the BESS scheduling problem permanently reduces the capacity of the lithium-ion cells [18]. The literature classifies ageing into cycle and calendar degradation. Cycle ageing refers to the reduction in cell performance recorded during cycling. The phenomenon is driven by stress factors such as depth-of-discharge (DoD), temperature, C-rate, cut-off voltages, and average state of charge (SoC) [19]. Several studies include cycle ageing models in the optimal scheduling of a BESS. [20] proposes a cycle ageing power law as a function of the depth of discharge (DOD) using a rainflow algorithm to compute the system cycles. In [21] authors assume battery degradation related to the DoD and SOC. Both variables have a non-linear relationship with the degradation of the system, and their contribution to the ageing is modelled with a novel one-dimensional linearisation technique using half cycles. In [22] authors exploit a logarithmic degradation function to implement an advanced rainflow counting algorithm. However, recent studies pointed out that the cycle ageing of lithium-iron phosphate (LFP) cells, which are the current industry standard thanks to their high cycle life and cost effectiveness [23], have a weak correlation with DoD [24]. Moreover, proper cell cooling shows that capacity fade is independent of the current rate up to 5C if the cell is kept within 20% and 80% of the SoC [25]. These findings enable the use of a throughput model to represent the cycle ageing of LFP cells. Building on this, [26] developed a multi-year planning and sizing algorithm for a rural microgrid incorporating a linear efficiency model and throughput-based cycle ageing, while [27] proposed a two-stage MILP framework for optimal BESS sizing in which SOH degradation is modelled as a function of charge and discharge cycles. Furthermore, considering only cycle ageing leads to an important approximation since the cells are also degraded by calendar ageing, which has a strong impact, especially in the first years of the cell's life [28,29]. In [30], the authors propose a MILP model that addresses both cycle and calendar ageing in V2G applications. The model can grasp the non-linear trends of ageing, stating that the neglect of the degradation in the operation may lead to an increase of 28% in the scheduling cost. However, the daily scheduling takes up to 1 min to define the schedule of a 24-hour optimisation without uncertainty, posing questions on the tractability of more complex problems. [31] proposes a complete ageing model accounting for cycle and calendar ageing pointing out the importance of the representations of these phenomena but uses a linear function for the dependency of calendar ageing with SoC. To summarise degradation-aware scheduling has advanced considerably, significant limitations remain. DoD-based cycle ageing models are well-established but poorly suited to LFP cells, which are increasingly dominant in real deployments, making throughput-based representations more appropriate. However, most scheduling studies apply these in isolation, neglecting calendar ageing despite its demonstrated impact in the early life of the cell. Where combined ageing models have been proposed [30,31] their computational cost raises tractability concerns even in deterministic settings, and neither has been extended to uncertainty-aware frameworks. These shortcomings, taken together with the efficiency modelling limitations discussed above, motivate the need for a unified, computationally tractable BESS model capturing both efficiency non-linearity and combined ageing effects within a scheduling framework capable of handling RES uncertainty.

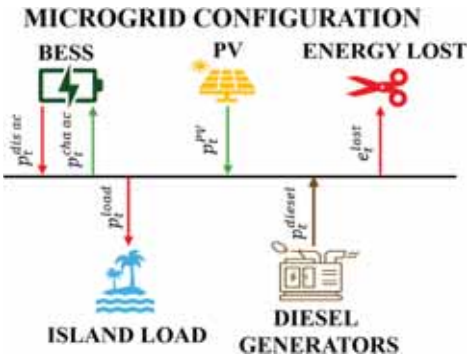

Fig. 1. Medium voltage isolated microgrid modelled in this paper.

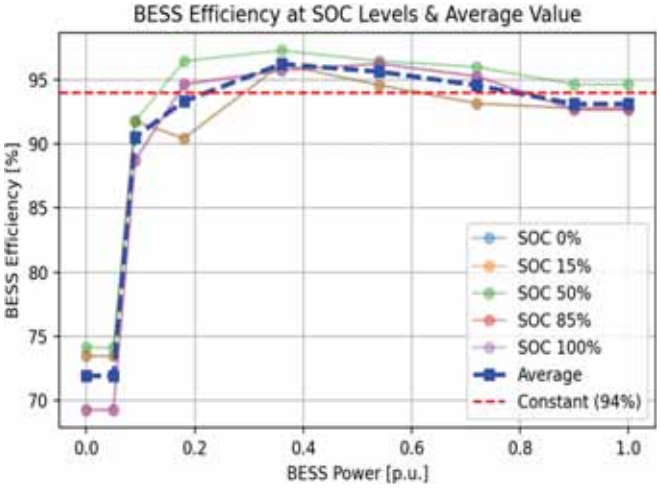

Fig. 2. BESS non-linear round-trip efficiency.

1.1. Novel contributions

Overall, the literature has separately investigated chance constrained spinning reserve scheduling, advanced BESS efficiency modelling, and degradation-aware optimisation. However, advanced BESS models have only been validated in deterministic scheduling problems because of their computational complexity. As summarized in Table 1 uncertainty-aware microgrid scheduling frameworks still rely on simplified battery representations based on constant efficiency and limited ageing modelling. This gap limits the development of realistic and computationally tractable scheduling tools for isolated microgrids with high RES penetration. This study develops a linearised model for BESS efficiency and calendar ageing by keeping the tractability of the optimisation model compact. According to the above discussion, the significant contributions of this paper are as follows:

- Advanced BESS modelling for scheduling: Although several advanced BESS models have been proposed in the literature, their formulations typically introduce additional binary variables to represent efficiency, limiting their applicability in complex optimisation problems. This work addresses this gap by incorporating an advanced BESS model based on the piecewise affine interpolation that uses only the charge and discharge binary variables in the scheduling procedure.
- Comprehensive ageing representation: A combined ageing model, incorporating both calendar and cycle ageing effects, is developed to provide a more realistic assessment of battery degradation over time. The ageing models are tuned with open-access data and are implemented in the MILP without the need for binary variables.
- Two isolated microgrid scheduling problems are developed to validate the advanced BESS model. The first consists of a yearly deterministic planning model that demonstrates the accuracy and low computational effort of the proposed BESS formulation. The second addresses short-term operation and integrates an established chance-constrained framework from the literature to handle spinning reserve uncertainty, enabling the evaluation of the advanced BESS model within a more complex optimisation problem.

The remainder of the paper is organised as follows. Section 2 presents the proposed methodology, beginning with the deterministic scheduling model for an isolated microgrid and proceeding to the linearization of the efficiency and ageing equations. It then introduces the chance-constrained scheduling algorithm for the isolated microgrid. Section 3 describes the real-world case study used to validate the proposed model. Section 4 reports and discusses the results, where the advanced BESS model is first validated with a deterministic optimisation and subsequently evaluated under uncertainty with the chance constrained modelling paradigm. Finally, Section 5 summarises the main findings and outlines directions for future work.

2. Methodology

The reference microgrid structure, as reported in Fig. 1, assumes an isolated system where loads, residential and industrial ones, are fed by diesel generators. The more and more important decarbonization target pushes for a strong use of RES; moreover, the energy and stability management of the microgrid could be easier by adopting a BESS.

The proposed isolated microgrid scheduling model aims to provide insight into the scheduling cost for the microgrid operator. The microgrid scheduling model is formulated as a MILP to determine the charging and discharging power of the BESS, as well as the power output of the diesel generators over two different time horizons. An advanced BESS formulation is developed to account for the efficiency and the cycle and calendar ageing. This formulation is first tested in a yearly deterministic planning horizon to test its performance. Furthermore, a chance-constrained approach is formulated to address the uncertainty of the spinning reserve and test the BESS model developed in a complex formulation.

2.1. Objective function

The objective function of the isolated microgrid scheduling model minimises the scheduling cost of the isolated microgrid. Eq. (1) details the objective function of the scheduling problem, where t denotes the scheduling time period, and g denotes the set of diesel generators.

$$\min\left(\sum_{t=1}^{T}\left(\sum_{g=1}^{N_g} p_{t,g}^{diesel}\pi^{diesel} + x_{t,g}^{start}\pi^{start}\right) + e_t^{lost}\pi^{cost}\right) \quad (1)$$

The objective function of the scheduling problem minimises the operation cost of the microgrid over T hours. The objective function accounts for the operational cost of the diesel generators, which includes the fuel cost (π^{diesel}) multiplied by the power produced by generator g ($p_{t,g}^{diesel}$) and the start-up cost (π^{start}) times the start-up binary variable for generator g ($x_{t,g}^{start}$). Furthermore, the modelling approach selected allows the microgrid to dissipate energy. The objective function includes this possibility with a penalisation cost (π^{cost}) representing the economic loss of the RES curtailment (e_t^{lost}). Eq. (2) describes the energy balance of the microgrid. The left side of the equality constraints represents the production with the PV power ($p_t^{PV\ kW}$), the diesel power, and the BESS discharge power ($p_t^{dis\ ac\ kW}$). The right side details the consumption of the electric load (p_t^{load}), the energy curtailed and the BESS charge power ($p_t^{cha\ ac\ kW}$).

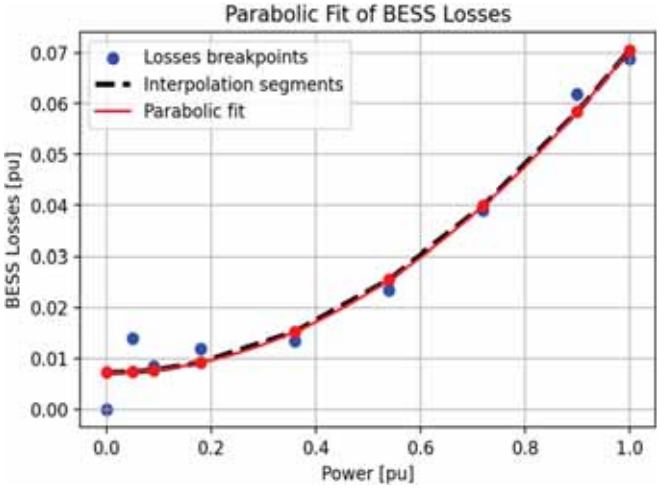

Fig. 3. Parabolic fit of the BESS losses. In blue, the losses obtained from the BESS efficiency, in red, the best parabolic fit for those points, and in black, the interpolating segments of the piecewise affine interpolation. (For interpretation of the references to color in this figure legend, the reader is referred to the web version of this article.)

Table 2
Input parameters for the piecewise affine BESS losses interpolation.

Segment	BESS power interval [p. u.]	Angular coefficient M_s^{losses}	Intercept Q_s^{losses}
1	[0.05, 0.09]	0.0030	0.0072
2	[0.09, 0.18]	0.0036	0.00741
3	[0.18, 0.36]	0.0082	0.00773
4	[0.36, 0.54]	0.0337	0.00922
5	[0.54, 0.72]	0.0567	0.0152
6	[0.72, 0.9]	0.0798	0.0255
7	[0.9, 1]	0.0185	0.0398

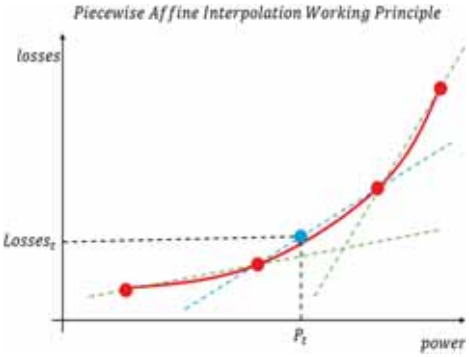

Fig. 4. Working principle of the piecewise affine interpolation method for MILP.

$$p_t^{PV\ kW} + p_t^{dis\ ac\ kW} + \sum_{g=1}^{N_g} p_{t,g}^{diesel} = p_t^{load} + p_t^{cha\ ac\ kW} + e_t^{lost} \quad (2)$$

Diesel generators are subject to operational constraints during the scheduling horizon, and their start-up costs are modelled through binary decision variables.

$$x_{t,g}^{diesel} P_{min}^{diesel} \le p_{t,g}^{diesel} \le x_{t,g}^{diesel} P_{max}^{diesel} \quad (3)$$

$$x_{t,g}^{start} \ge x_{t,g}^{diesel} - x_{t-1,g}^{diesel} \quad (4)$$

Eq. (3) imposes the minimum (P_{min}^{diesel}) and maximum (P_{max}^{diesel}) power limits for each diesel generator with an on/off binary variable ($x_{t,g}^{diesel}$). Eq. (4) enforces the generator start-up logic with the time differential between the on/off diesel binary variables.

2.2. BESS modelling in MILP

This section introduces a MILP-based formulation to efficiently linearise the BESS efficiency. Fig. 2 shows the round-trip efficiency of an NMC BESS developed in [38] as a function of power and SoC. As stated in [17], the dependency of the system efficiency on SOC is negligible. Therefore, the BESS model developed focuses on accurately representing the dependency of the BESS performances in a MILP as a function of the power. Each point on the dashed blue curve represents the BESS efficiency averaged over different SoC levels at the same power. The breakpoints of the blue curve are the inputs used to develop the advanced BESS model. Each breakpoint is a function of the BESS power $efficiency_k = f(P_k^{BESS})$. The figure also depicts a constant BESS efficiency value of 94%, useful as a term of comparison in the validation procedure.

The linearization of the efficiency breakpoints is performed using the piecewise affine interpolation technique described in [39]. This technique is a specific convex piecewise linear approximation in which the active segment is implicitly selected through linear inequality constraints, without introducing additional binary variables or special order sets (SOS) constraints, which are effective in small-scale or short-term problems, but scales poorly with the number of time steps. This feature is particularly relevant for the proposed formulation, since the model is applied to a full-year horizon and then integrated in a chance-constrained problem, where preserving a compact MILP structure is of primary importance.

Since the efficiency function adopted is non-convex, it must first be transformed into a convex function to apply this technique. The conversion of the efficiency into the BESS losses generates a convex function. The BESS losses function can be linearised and inserted in the MILP formulation to model the variable efficiency as a function of the BESS power. Eq. (5) converts the efficiency function into the BESS losses function for every breakpoint of the curve.

$$losses_k = \left(P_k^{BESS} - efficiency_k * P_k^{BESS}\right) = f\left(P_k^{BESS}\right) \quad (5)$$

The equation converts the efficiency value associated with a P_k power breakpoint into the BESS power losses ($losses_k$). However, as shown in Fig. 3, the distribution of the blue point, which represents the outcome of Eq. (5), is not convex yet. A quadratic regression transforms the blue dots' distribution into a convex MILP tractable formulation. This last step enables the linearisation with the piecewise affine interpolation techniques. The red line shown in Fig. 3 is the quadratic regression of the blue point distribution and is the function linearised by the piecewise affine interpolation.

The linearization of the BESS losses function allows for representing the efficiency of the BESS inside the MILP formulation. The piecewise affine interpolation uses a set of segments (black dashed line in Fig. 3) with different angular coefficients and intercepts to linearise a convex function. Therefore, a fundamental step is the computation of the angular coefficient and the intercept of each line from the quadratic regression. We divided the quadratic functions into K breakpoints and $S = K - 1$ segments. Given the coordinates of each breakpoint ($power_k$, $losses_k$) Eq. (6) compute the angular coefficient, and Eq. (7) defines the intercept of the interpolating lines between each breakpoint.

$$M_s^{losses} = \frac{losses_k - losses_{k-1}}{power_k - power_{k-1}} \quad (6)$$

$$Q_s^{losses} = losses_k - M_s^{losses} * P_k^{BESS} \quad (7)$$

The angular coefficient (M_s^{losses}) and the intercept (Q_s^{losses}) are inputs of the optimisation and enable the implementation of the piecewise affine interpolation to linearise the power losses function. The set of Eqs. (8)

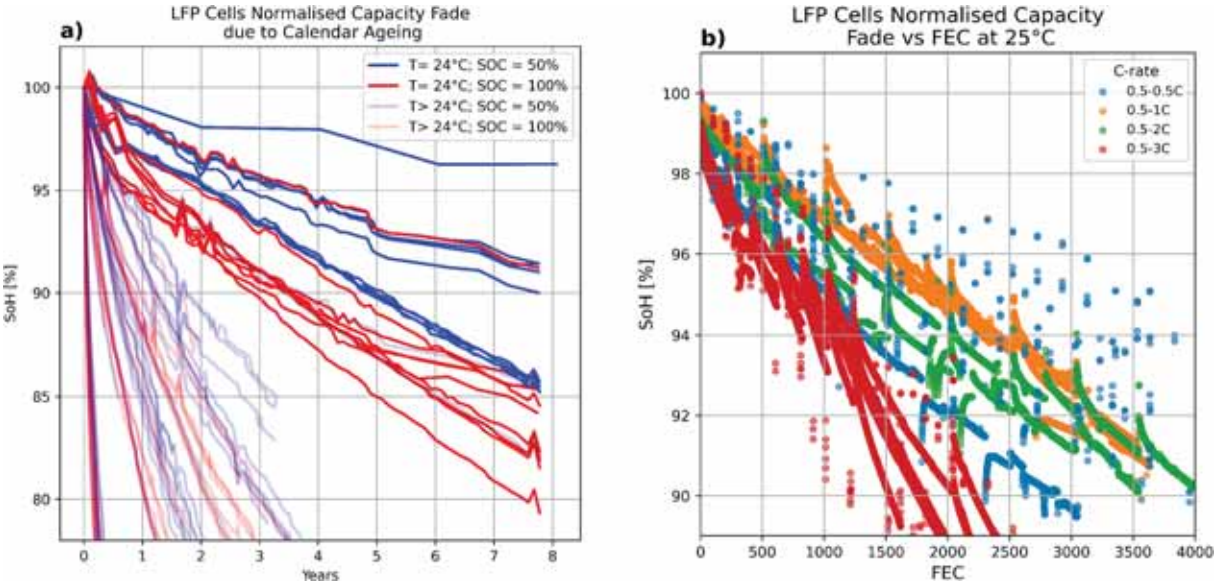

Fig. 5. Calendar (a) and cycle (b) ageing open access data used as input for the BESS degradation function implemented in the MILP model.

and (9) imposes the piecewise affine interpolation approach to the BESS charge and discharge losses inside the optimisation.

$$Losses_t^{cha} \geq M_s^{losses}\left(p_t^{cha\ ac} - P_k\right) + Q_s^{losses} * z_t^{cha} \tag{8}$$

$$Losses_t^{dis} \geq M_s^{losses}\left(p_t^{dis\ ac} - P_k\right) + Q_s^{losses} * z_t^{dis} \tag{9}$$

Table 2 summarises the input parameters of the losses piecewise affine interpolation. Each segment is characterised by an angular coefficient and an intercept, defined between two consecutive breakpoints. It is worth noting that the angular coefficients follow a monotonically increasing trend, and that the breakpoint P_k adopted in Eqs. (8) and (9) corresponds to the first breakpoint of the respective segment.

Fig. 4 illustrates in detail the working principle of the piecewise affine interpolation method. The inequality constraints expressed by Eqs. (8) and (9), determine the charge and the discharge losses at each optimisation time instant *t*. The losses are higher than or equal to the maximum values computed by the input segments (*s*) with the AC per unit power identified by the optimisation. The solver evaluates the values obtained with the s segments (shown as dashed lines). Since the loss function is convex, the segment in which the AC per unit power identified by the optimisation lies (highlighted in light blue) is always above the other segments (shown in green). Therefore, the adopted constraint ensures that the BESS losses are equal to or higher than the highest value obtained by the s segments. Since the highest segment is always the one between the breakpoints in which the power falls, the losses are interpolated without the need for binary variables. The only binary variables required by this formulation are z_t^{cha}, z_t^{dis} related to the operational dichotomy of the BESS that sets the charge losses equal to zero when the BESS is discharging and sets the discharge losses equal to zero when the BESS is charging.

The formulation described above efficiently linearises the power losses function, and it works properly in a minimisation problem. To ensure the correct implementation of the technique, it is necessary to insert a penalisation weight in the objective function. The penalisation weights adopted are the charge and the discharge losses. The piecewise affine interpolation constraints and the penalisation factors bound the losses on the interpolating segments. Finally, the model also incorporates the following constraints to operate the BESS in line with its working principle.

$$p_t^{cha\ ac} = p_t^{cha\ dc} + Losses_t^{cha} \tag{10}$$

$$p_t^{dis\ ac} = p_t^{dis\ dc} - Losses^{dis} \tag{11}$$

$$p_t^{dis\ ac} \leq z_t^{dis} \tag{12}$$

$$p_t^{cha\ ac} \leq z_t^{cha} \tag{13}$$

$$z_t^{cha} + z_t^{dis} \leq 1 \tag{14}$$

$$p_t^{cha\ ac\ kW} = p_t^{cha\ ac} * P_{nom}^{BESS} \tag{15}$$

$$p_t^{dis\ ac\ kW} = p_t^{dis\ ac} * P_{nom}^{BESS} \tag{16}$$

$$E_t = E_{t-1} + \left(p_t^{cha\ dc} - p_t^{dis\ dc}\right) * P_{nom}^{BESS} \tag{17}$$

$$SOC_t = \frac{E_t}{E_{nom}^{BESS}} \tag{18}$$

Eq. (10) defines the charging power balance, equating the AC-side charging power to the sum of the DC-side charging power and the losses obtained with the piecewise affine interpolation. Eq. (11) represents the dual case, where the AC-side discharging power is expressed as the difference between the DC-side discharging power and the losses. Eqs. (12), (13), and (14) enforce the operational dichotomy of the BESS: the per-unit AC power cannot exceed unity, and the binary variables governing the charge and the discharge phase cannot be simultaneously active. To maintain the system's energy balance, Eqs. (15), and (16) convert per-unit power into the physical values used in the energy balance in Eq. (2). Eq. (17) describes the temporal evolution of the system's energy, while Eq. (18) relates the internal energy of the BESS to its SOC. The next sections specify the BESS SOC boundaries that are a function of the capacity fade model developed in this work.

Lastly, to validate the model's performance, the mean absolute error (MAE) expressed by Eq. (19) is used.

$$\boldsymbol{MAE}^{\boldsymbol{BESS}} = \frac{1}{\boldsymbol{T}} \sum_{t=1}^{T} \left| \boldsymbol{Eff}_{\boldsymbol{MILP}} - \boldsymbol{Eff}_{\boldsymbol{LUT}}\left(\boldsymbol{P}^{\boldsymbol{BESS}}, \boldsymbol{SoC}^{\boldsymbol{BESS}}\right) \right| \tag{19}$$

The charge and discharge efficiency computed from the losses of the MILP model (Eff_{MILP}) is benchmarked with the look-up table efficiency (Eff_{LUT}) shown in Fig. 2. Since the LUT efficiency is a function of the AC power and the SoC, we computed its value with a linear interpolation. The AC charge or the AC discharge with the SoC defined by the

Table 3
input parameters for the piecewise affine calendar ageing interpolation.

Segment	SoC interval [%]	Angular coefficient M_a^{ageing}	Intercept Q_a^{ageing}
1	[0, 50]	0	0.00191
2	[50, 100]	0.00169	0.00191

optimisation are the inputs of the linear interpolation that define the efficiency benchmark using these two values. The MAE evaluates all the efficiency values obtained when the BESS has an AC power higher than 0.05 per unit.

2.3. Cell degradation models

A further novelty of the BESS model proposed is represented by the implementation of an online capacity fade model. The procedure uses open access ageing data to generate cycle and calendar ageing trends to insert into the BESS model. These trajectories are linearised and inserted in the MILP formulation to enable the ageing of the system within the optimisation framework. The energy-to-power ratio (EPR) of BESS installed in the electric power system is increasing [40]. It follows that the presence of a high C-rate will be improbable, and with the installation of a liquid-cooled auxiliary system, the temperature of the cells within a BESS will always be kept within 20 °C and 30 °C, limiting temperature transient and consequent degradation [41]. Therefore, under these conditions, the influence of C-rate and temperature on capacity fade of utility-scale BESS can be considered limited and is not explicitly modelled. It should be noted that any deviation from this operational envelope, such as sustained high C-rates or inadequate thermal management, may lead to an increase in overall capacity fade beyond what is estimated by the proposed model. This aspect is acknowledged as a boundary condition of the current formulation, and its explicit quantification is left for future work.

The calendar ageing model uses the data published by a research group of Stanford [42] to define a trajectory as a function of the SoC. The cycle ageing model has been assumed function of the full equivalent cycles (FEC) and is tuned thanks to the database shared by the Sandia National Laboratories (SNL) in [24] and publicly available in [43]. Fig. 5a depicts the calendar ageing trajectories recorded at Stanford. The bold trends in the figure represent the data used as input for the calendar ageing model. Fig. 5b reports the cycle ageing trends gathered from the SNL publicly available database.

The methodology adopted to create the calendar ageing model uses as input the LFP calendar ageing trajectories at 24 °C at different SoC levels. The capacity fade trends at the same SoC level are averaged to obtain a unique value that is fitted in the expression defined by Eq. (20).

$$\boldsymbol{C_{fade}^{calendar}t = A(SoC)_t * \sqrt{t}} \tag{20}$$

The expression links the capacity fade generated by calendar ageing with the square root of time. This assumption is widely adopted in the literature to describe the growth of the solid electrolyte interphase, which is the main calendar ageing driver [44].

To separate the cycle and calendar ageing contribution, a proper procedure has been developed. Assuming that cycle and calendar ageing phenomena linearly superimpose as discussed in [45], the calendar ageing model has been compared with the SNL data to isolate the cycle ageing contribution. The input data used to identify this trend comes from the test run at 25 °C with a C-rate below 1C. Since the cells have been cycled around 50%, the calendar ageing model at SOC equal to 50% is used to isolate the capacity fade trajectory related to cycling. The SNL degradation trajectories at 1C and 25 °C are firstly normalised at the cell nominal capacity. The average of the normalised curve is used to extrapolate the cycle ageing trend. The selected calendar ageing trend is added to the cycle ageing normalised curve to isolate the contribution of the cycle ageing to the capacity fade. The resulting trends are averaged and fitted with the linear expression described by Eq. (21).

$$\boldsymbol{C_{fade}^{cycle} = B * FEC} \tag{21}$$

Based on the assumptions made, the only issue to address is the linearization of the relationship between the calendar ageing and the BESS SoC. As demonstrated in Section 2.2, piecewise affine interpolation effectively linearises the convex functions. Therefore, this solution has been adopted to linearise the relationship between SoC and calendar ageing.

$$\boldsymbol{A(SoC)_t \geq M_a^{ageing}(SoC_t - SoC_a) + Q_a^{ageing}} \tag{22}$$

$$\boldsymbol{C_{fade_t}^{calendar} = A(SoC) * Time_t^{ageing}} \tag{23}$$

$$\boldsymbol{Time_t^{ageing} = \sqrt{t + T_0} - \sqrt{t - 1 + T_0}} \tag{24}$$

$$\boldsymbol{C_{fade_t}^{cycle} = B * \frac{P_t^{dis\ dc} + P_t^{cha\ dc}}{2}} \tag{25}$$

$$\boldsymbol{C_{fade_t} = C_{fade_t}^{cycle} + C_{fade_t}^{calendar}} \tag{26}$$

$$\boldsymbol{SoH_t = SoH_{t-1} - C_{fade}} \tag{27}$$

$$\boldsymbol{SoC_t \leq 1 - \frac{1 - SoH_t}{2}} \tag{28}$$

$$\boldsymbol{SoC_t \geq \frac{1 - SoH_t}{2}} \tag{29}$$

Eq. (22) applies the piecewise affine interpolation to compute the coefficient that rules the relationship between SoC and calendar ageing. This variable is used in Eq. (23) to generate the calendar ageing trajectories inside the optimisation. The parameter ($Time_t^{ageing}$) expresses the square root contribution of time to the calendar ageing. Its value is expressed by Eq. (24), where T_0 defines the calendar life of the cell. As a comprehensive experimental characterisation of calendar ageing at continuously variable SoC levels is not yet available in the literature, the proposed model interpolates the calendar ageing contribution within the envelope defined by the trends identified at 0%, 50% and 100% SoC, ensuring physical consistency with the experimental evidence. Eq. (25) uses the cycle ageing coefficient identified to compute the cycle ageing in a given optimisation instant. Eq. (26) linearly superposes the cycle and the calendar ageing in a given time instant. Although the linear superposition is an approximation, as demonstrated in [46], this assumption is widely adopted in the literature for BESS techno-economic analysis [37,47–49]. Eq. (27) updates the state of health (SoH) of the BESS. Eqs. (28) and (29) reduce the available BESS capacity every time instant as a function of the cycle and the calendar ageing trends identified. The SoC boundaries are therefore defined over the dynamically evolving usable capacity, rather than the nominal one. The initial bounds of 0% and 100% are thus consistent with this formulation, as the Battery Management System continuously accounts for the current SoH of the BESS, preventing system deep discharge or overcharge.

Table 3 summarises the input parameters of the calendar ageing piecewise affine approximation. The two segments have an angular coefficient and an intercept, defined between two consecutive breakpoints.

Furthermore, to clarify the impact that the calendar ageing angular coefficients and intercept have on the optimisation, the validation procedure of the BESS model presented in the next section includes a sensitivity analysis. The sensitivity analysis compares the BESS model with the base coefficients reported in Table 3 with nine additional configurations with different calendar ageing trends. The ultimate goal is to evaluate the impact that different coefficients have on the ageing of the asset and on the objective function. Similar to the base configuration, each new configuration has three calendar ageing breakpoints

Table 4
Breakpoints and consequent coefficients for the calendar ageing sensitivity analysis.

Model	Calendar ageing breakpoints SoC_a	Angular coefficient M_a^{ageing}	Intercept Q_a^{ageing}
Model 1	[0.0015, 0.0015, 0.0024]	[0, 0.0018]	[0.0015, 0.0015]
Model 2	[0.0015, 0.0015, 0.0028]	[0, 0.0026]	[0.0015, 0.0015]
Model 3	[0.0015, 0.0015, 0.0033]	[0, 0.0033]	[0.0015, 0.0015]
Model 4	[0.0015, 0.00175, 0.0024]	[0.0005, 0.001358]	[0.0015, 0.00175]
Model 5	[0.0015, 0.00175, 0.0028]	[0.0005, 0.0021]	[0.0015, 0.00175]
Model 6	[0.0015, 0.00175, 0.0033]	[0.0005, 0.003256]	[0.0015, 0.00175]
Model 7	[0.0015, 0.00225, 0.00242]	[0.0015, 0.0035]	[0.0015, 0.00225]
Model 8	[0.0015, 0.00225, 0.0028]	[0.0015, 0.0016]	[0.0015, 0.00225]
Model 9	[0.0015, 0.00225, 0.0033]	[0.0015, 0.0022]	[0.0015, 0.00225]

defined at SoC levels of 0, 50, and 100%, respectively. We selected the breakpoints based on the calendar ageing test results reported in [42] ensuring broad exploration of possible calendar ageing trends for a BESS. Table 4 lists the calendar ageing breakpoints and the angular coefficients and intercepts obtained from those breakpoints and adopted in the sensitivity analysis.

2.4. Chance-constrained spinning reserve

In a microgrid, such as the one adopted in this paper, it is necessary to maintain energy balance and provide an adequate spinning reserve to guarantee both steady-state and transient stability. As pointed out in Section 1.1, the well-established chance-constrained optimisation model proposed in [11] is adopted to assess the performance of the advanced BESS model proposed. The focus of this section is to analyse the behaviour and effectiveness of the proposed BESS formulation when embedded within a probabilistic scheduling framework.

The probabilistic spinning reserve is a fundamental input for the chance-constrained optimisation model. In the adopted MILP formulation, the spinning-reserve requirement of the isolated microgrid is expressed as a probabilistic constraint. This constraint ensures that the available spinning reserve (SR_t) is greater than or equal to the possible realisations of the reserve demand ($P_{t,w}$) with a probability equal to or higher than a confidence level α as expressed by Eq. (30).

$$\boldsymbol{Prob}\{\boldsymbol{SR}_t > \boldsymbol{P}_{t,w}\} > \boldsymbol{\alpha} \tag{30}$$

It follows that the chance-constrained formulation requires, as input, a set of parameters that describe both the probability of occurrence of each spinning-reserve magnitude and the corresponding reserve levels. Consequently, the procedure presented in this section describes the development of an hourly discrete probability density function for both upward and downward spinning reserve.

Clustering or scenario reduction methods can simplify computation, but may distort the distribution of net load uncertainty, particularly in the tail regions that are crucial for reserve adequacy. Hence, the load and the PV annual profile were used in their entirety to generate the spinning reserve probability density function [50]. These parameters are used to compute the residual load at each hour t as expressed in Eq. (31).

$$\boldsymbol{L}_t^{residual} = \boldsymbol{p}_t^{load} - \boldsymbol{p}_t^{PV} \tag{31}$$

The spinning reserve must compensate for fluctuations in the residual load to respond to unexpected changes in demand and the variability of generation. The residual load differential (L_t^{diff}) computed using Eq. (32) provides an appropriate representation of the spinning reserve requirements of the microgrid [51].

$$\boldsymbol{L}_t^{diff} = \boldsymbol{L}_t^{resiudeal} - \boldsymbol{L}_{t-1}^{residual} \tag{32}$$

The load differential, which represents the spinning reserve requirement in a given hour, assumes both positive and negative values. To distinguish between upward and downward reserve, the positive values are assigned to the upward spinning reserve distribution (sp_t^{up}), while the negative values go into the downward reserve distribution (sp_t^{down}). This classification allows the construction of distinct distributions for upward and downward spinning reserves.

For each hour, the hourly spinning reserve values obtained from the residual load differential are used to estimate the upward and downward probability density functions (pdf_t^{up},pdf_t^{down}) of every hour. A total of 48 probability density functions are developed. Since probability density functions are continuous, they cannot be directly embedded in the optimisation framework. Therefore, a discretisation procedure is applied, transforming each continuous probability density function into a discrete distribution with *Ns* intervals. To build the discrete distribution for a given hour, the probability density function is divided into Ns + 1 bins. Each interval, spanning from the minimum to the maximum observed spinning reserve value in the hour under evaluation, is characterised by two parameters: the reserve magnitude defined as the average spinning reserve value within the interval s ($E_{t,s}^{res\ up}$, $E_{t,s}^{res\ down}$), and its probability of occurrence, computed as the sum of the probabilities falling within the interval ($Prob\left(E_{t,s}^{res\ up}\right)$, $Prob\left(E_{t,s}^{res\ down}\right)$).

The discrete probability density functions obtained are the input parameters for the chance-constrained optimisation model discussed in the subsequent section. The spinning reserve is crucial to the level of the fluctuating power outputs of intermittent RES and ensuring a reliable and economic operation of the system. To provide an adequate spinning reserve, it is necessary to estimate the upward and downward reserve of the dispatchable units installed in the microgrid: diesel generators and BESS.

$$\boldsymbol{SR}_{t.g}^{up\ diesel} \le \boldsymbol{P}_{max}^{diesel}\boldsymbol{x}_{t.g}^{diesel} - \boldsymbol{p}_{t.g}^{diesel} \tag{33}$$

$$\boldsymbol{SR}_{t.g}^{down\ diesel} \le \boldsymbol{p}_{t.g}^{diesel} - \boldsymbol{p}_{min}^{diesel}\boldsymbol{x}_{t.g}^{diesel} \tag{34}$$

$$\boldsymbol{SR}_t^{up\ BESS} \le \boldsymbol{P}_{nom}^{BESS} + \boldsymbol{p}_t^{cha\ kW} - \boldsymbol{p}_t^{dis\ kW} \tag{35}$$

$$\boldsymbol{SR}_t^{up\ BESS} \le \boldsymbol{E}_t^{BESS} \tag{36}$$

$$\boldsymbol{SR}_t^{down\ BESS} \le \boldsymbol{P}_{nom}^{BESS} - \boldsymbol{p}_t^{cha} + \boldsymbol{p}_t^{dis} \tag{37}$$

$$\boldsymbol{SR}_t^{down\ BESS} \le \boldsymbol{E}_{nom}^{BESS} - \boldsymbol{E}_t^{BESS} \tag{38}$$

$$\boldsymbol{SR}_t^{up} = \boldsymbol{SR}_t^{up\ BESS} + \sum_{g=1}^{N_g} \boldsymbol{SR}_{t.g}^{up\ diesel} \tag{39}$$

$$\boldsymbol{SR}_t^{down} = \boldsymbol{SR}_t^{down\ BESS} + \sum_{g=1}^{N_g} \boldsymbol{SR}_{t.g}^{down\ diesel} \tag{40}$$

Eqs. (33) and (34) define the feasible ranges of upward and downward spinning reserves for each diesel generator; the reserve for these assets is equal to the difference between the generator's technical limits and its current operating point. Constraint (35) limits the BESS upward spinning reserve to a value no greater than its nominal power plus the net charging capability, i.e., the difference between charging and discharging power at the current time. Furthermore, constraint (36) further bounds the BESS upward spinning reserve according to the amount of energy currently stored in the system. Additionally, constraints (37) and (38), determine the downward spinning reserve through the dual formulation of the upward spinning reserve. Finally, for clarity, constraints (39) and (40) define the microgrid's upward and downward

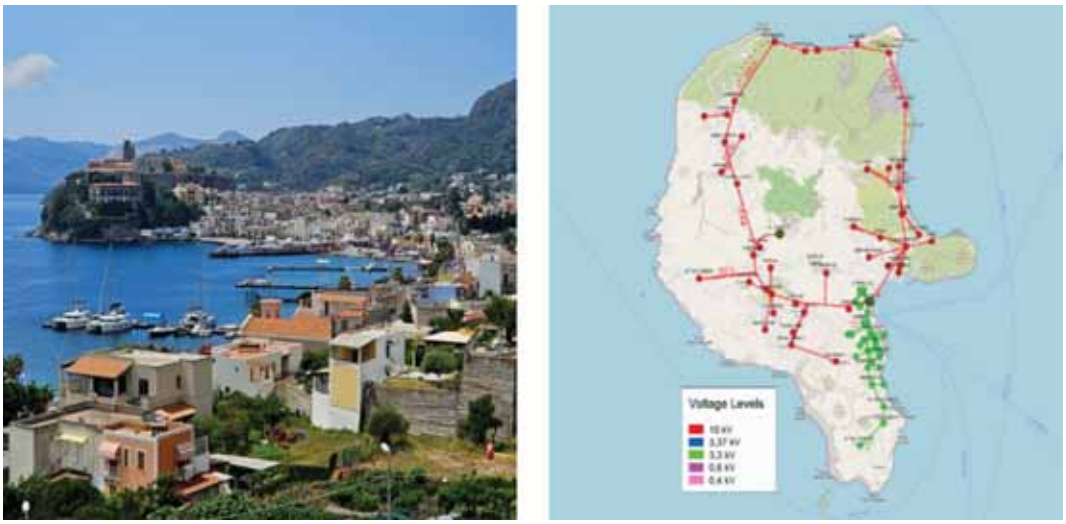

Fig. 6. Photos of Lipari Island.

spinning reserves as the sum of the contributions from all dispatchable units.

Chance-constrained programming is a mathematical optimisation framework that incorporates probabilistic constraints to account for uncertainty. Eq. (41) specifies the probability constraint used to ensure that the microgrid consistently satisfies the upward spinning reserve requirements.

$$\boldsymbol{Prob}\left\{\boldsymbol{SR}_t^{up} \geq \boldsymbol{E}\left(\boldsymbol{E}_t^{res\ up}\right)\right\} \geq \boldsymbol{\alpha} \tag{41}$$

Here, α is an input parameter, referred to as the confidence level, which specifies the probability that the constraint will be satisfied. Whilst $E\left(E_t^{res\ up}\right)$ is the expected value of the upward spinning reserve. The constraint requires that the upward spinning reserve be greater than or equal to the expected spinning reserve requirement for at least a proportion of time equal to α. This probabilistic constraint is nonlinear and cannot be directly handled by MILP. To linearise it and render it tractable, the methodology proposed in [39] is applied. To transform the chance-constrained problem indicated in Eq. (41) into a deterministic form, it is necessary to introduce a new binary variable $W_{t,w}$ which satisfies the following if-else condition.

$$\boldsymbol{W}_{t,w}^{up} = \begin{cases} \boldsymbol{1\ if\ SR}_t^{up} \geq \boldsymbol{E}_{t,w}^{res\ up} \\ \boldsymbol{0\ otherwise} \end{cases} \tag{42}$$

Eq. (42) requires that, for any period t, the variable $W_{t,s}$ equals 1 if and only if the upward spinning reserve is greater than or equal to the spinning reserve in interval s; otherwise, it equals 0. The parameter $E_{t,s}^{res\ up}$, defined along the set s, correspond to the magnitudes of the discrete probability function of the spinning reserve. Consequently, the constraint expressing that the upward spinning reserve of the microgrid at time instant t surpasses the expected spinning reserve with a probability higher than or equal to α can be linearized as follows.

$$\sum_{w=1}^{N_w} \boldsymbol{W}_{t,w}^{up} * \boldsymbol{Prob}\left(\boldsymbol{E}_{t,w}^{res\ up}\right) \geq \boldsymbol{\alpha} \tag{43}$$

$$\frac{\boldsymbol{SP}_t^{up} - \boldsymbol{E}_{t,w}^{res\ up}}{\boldsymbol{\tau}} \leq \boldsymbol{W}_{t,w}^{up} \leq \boldsymbol{1} + \frac{\left(\boldsymbol{SP}_t^{up} - \boldsymbol{E}_{t,w}^{res\ up}\right)}{\boldsymbol{\tau}} \tag{44}$$

Eq. (43) enforces that the summation over w of the product between the binary variable $w_{t,s}^{up}$ and the probability associated with a given magnitude of spinning reserve $Prob\left(E_{t,s}^{res\ up}\right)$ is greater than or equal to α. Eq. (44) guarantees that the binary variable $w_{t,s}^{up}$ takes a value of one when the spinning reserve exceeds the threshold defined by the value $E_{t,s}^{res\ up}$ of the discrete probability distribution of the spinning reserve. Here, τ denotes a large positive number, selected as a sufficiently large positive constant to deactivate the constraint when the condition is not satisfied. In this work, τ is defined equal to the 10 MW which is always greater than the maximum upward/downward spinning reserve achievable by the microgrid. This results in a value of the same order of magnitude as the system nominal power, thus avoiding excessively large coefficients. When the system's upward spinning reserve is greater than or equal to the upward spinning reserve in scenario s, Eq. (44) reduces to $\varepsilon \leq W_{t,s}^{up} \leq 1 + \varepsilon$. Since $W_{t,s}^{up}$ is a binary variable, this condition enforces the variable to 1. Conversely, if the condition is not satisfied, the inequality becomes $-\varepsilon \leq W_{t,s}^{up} \leq 1 - \varepsilon$, which forces the binary variable to zero. Eqs. (45) and (46) apply the procedure just explained to linearise the probabilistic constraint of the downward spinning reserve.

$$\sum_{w=1}^{N_w} \boldsymbol{W}_{t,w}^{down} * \boldsymbol{Prob}\left(\boldsymbol{E}_{t,w}^{res\ down}\right) \geq \boldsymbol{\alpha} \tag{45}$$

$$\frac{\boldsymbol{SP}_t^{down} - \boldsymbol{E}_{t,w}^{res\ down}}{\boldsymbol{\tau}} \leq \boldsymbol{W}_{t,s}^{down} \leq \boldsymbol{1} + \frac{\left(\boldsymbol{SP}_t^{down} - \boldsymbol{E}_{t,w}^{res\ down}\right)}{\boldsymbol{\tau}} \tag{46}$$

The proposed chance constrained MILP formulation is summarized as follows.

$$\boldsymbol{O.F.}\quad (\boldsymbol{1}) + \sum_{t=1}^{T}\left(\boldsymbol{losses}_t^{cha} + \boldsymbol{losses}_t^{dis} + \boldsymbol{A}(\boldsymbol{SoC})_t\right)$$

$$\boldsymbol{s.t.}$$

$$\boldsymbol{BESS\ constraints}: \boldsymbol{from}\ (\boldsymbol{8})\ \boldsymbol{to}\ (\boldsymbol{18})$$

$$\boldsymbol{microgrid\ constraints}: \boldsymbol{from}\ (\boldsymbol{2})\ \boldsymbol{to}\ (\boldsymbol{4})$$

$$\boldsymbol{spinning\ reserve}: \boldsymbol{from}\ (\boldsymbol{33})\ \boldsymbol{to}\ (\boldsymbol{40})\&\boldsymbol{from}\ (\boldsymbol{43})\ \boldsymbol{to}\ (\boldsymbol{46})$$

The terms in the objective function are penalisation factors used to ensure the correct implementation of the piecewise affine interpolation. Their impact on the formulation is deemed negligible and is confirmed in the results section. The deterministic planning scheduler used to validate the BESS relies on this objective function, incorporates the BESS constraints, and assumes a single diesel generator operating as a slack unit to limit the number of binary variables and maintain the computational tractability of the annual simulation.

Lasty we developed a key performance index to estimate the impact of the BESS size and the confidence level on the chance constrained formulation with a sensitivity analysis. Eq. (47) introduces the microgrid relative cost ($R_{Microgrid}$).

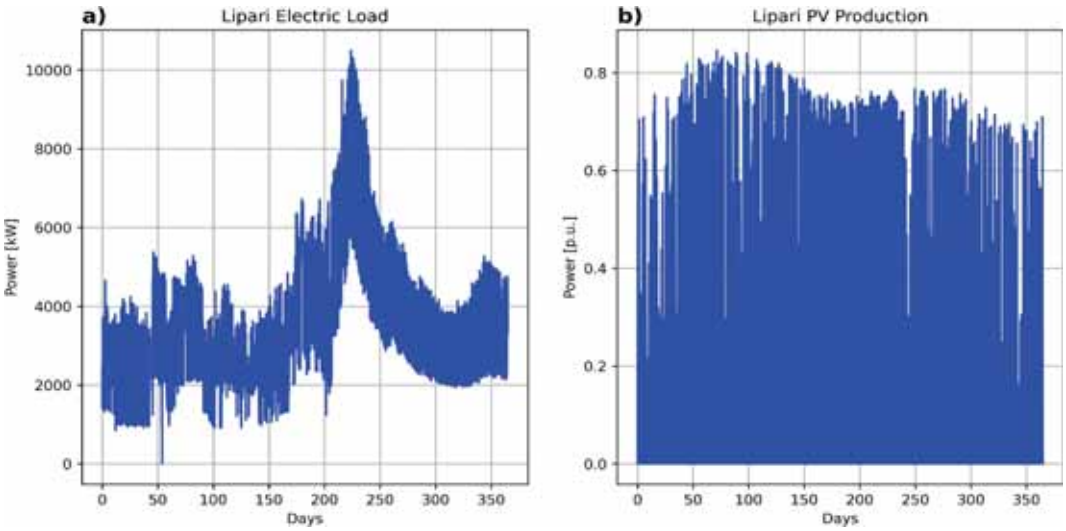

Fig. 7. Hourly load (a) and PV (b) profiles adopted as input for the proposed algorithm.

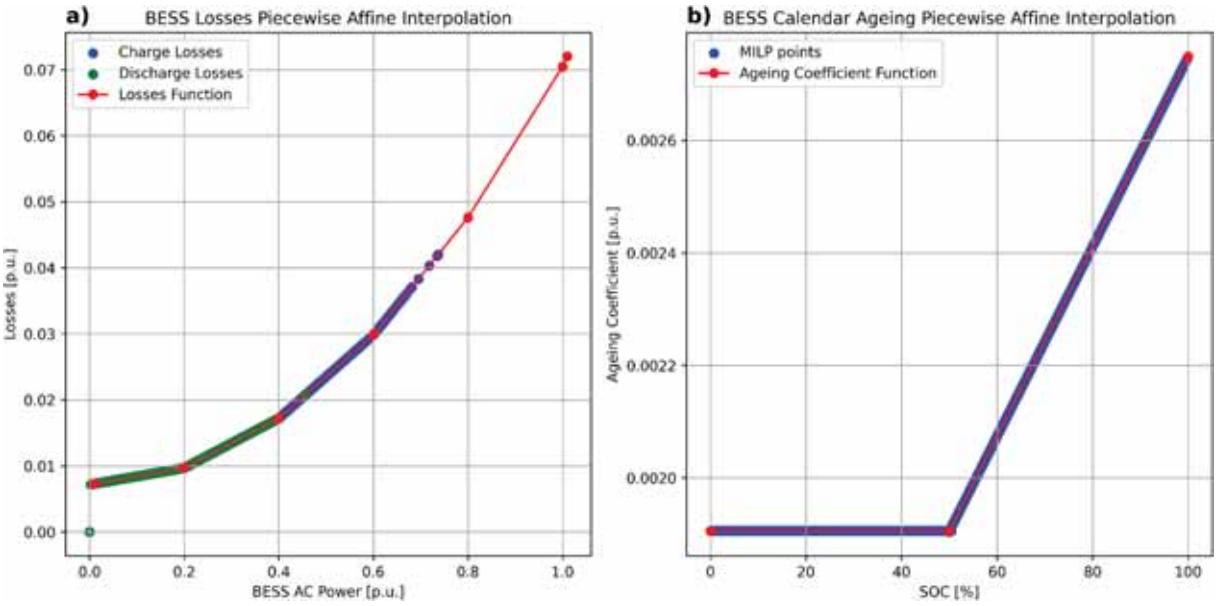

Fig. 8. charge and discharge losses (a) and calendar ageing coefficient (b) values interpolated with the piecewise affine algorithm in the optimisation.

$$R_{Microgrid} = 100^{*}\frac{MG^{cost}\left(P_{nom}^{BESS}, E_{nom}^{BESS}, \alpha\right)}{MG^{cost}\left(P_{nom}^{BESS}, E_{nom}^{BESS}, 0\right)} \quad (47)$$

The numerator of the proposed index represents the operating cost of the microgrid for a given BESS nominal power, nominal energy, and confidence level. This value is normalised by a benchmark microgrid cost ($MG^{cost}\left(P_{nom}^{BESS}, E_{nom}^{BESS}, 0\right)$), defined as the operating cost of the microgrid with a given BESS size installed and a confidence level equal to zero.

3. Case study

The objective of the optimisation models developed is to determine the optimal BESS scheduling of an isolated microgrid, given a specified PV nominal power and a desired confidence level for the spinning reserve uncertainty. The proposed tool defines the power profiles taking into account fundamental BESS parameters such as efficiency, cycle and calendar ageing.

To validate the approach and to ensure a practical application, the solution has been applied to a real case study: the Lipari microgrid. Lipari is both a geographical and an electrical island located approximately 25 km northeast of the Sicilian coast. The grid is operated by 13 diesel generators with an apparent power of approx 2 MVA each. Currently, the microgrid has a total of 1.7 MW of PV installed, but the decarbonisation target is driving the installation of new distributed power plants. This condition drives the needs of a BESS that is currently under evaluation and a proper scheduling algorithm to enhance its operation. Fig. 6 gives some glimpses of the Island and the structure of the local electric grid.

Società Elettrica Liparese (SEL), the distribution system operator (DSO) responsible for the microgrid, provided the load profile of Lipari Island in 2023. The PV generation data, normalised in per-unit values to ensure applicability across multiple case studies, was obtained from Renewable Ninja [52] (Fig. 7).

Table 4 summarises the input parameters of the isolated microgrid scheduling model.

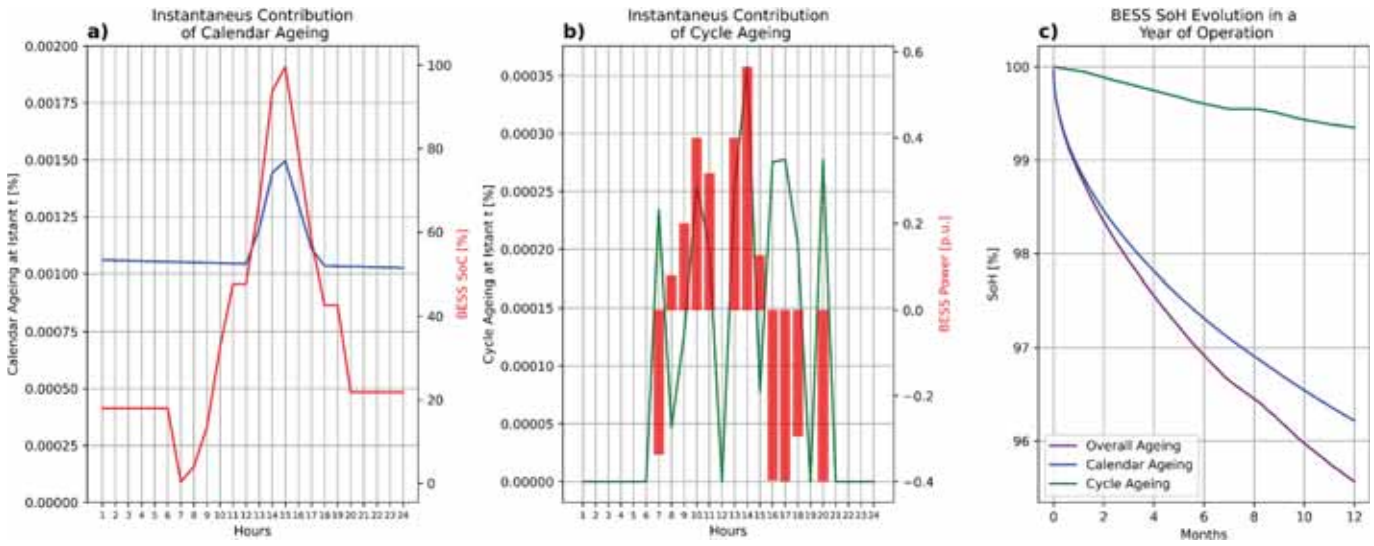

Fig. 9. Calendar (a) and cycle ageing (b) contribution to the BESS capacity fade in a day, and overall capacity fade computed during the optimisation (c).

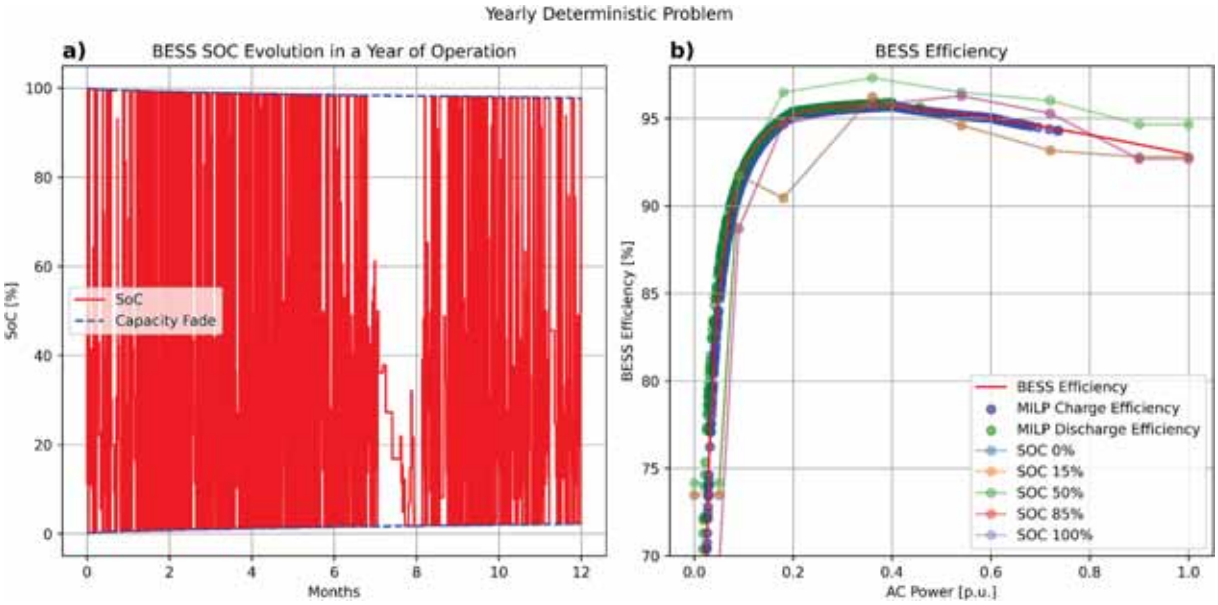

Fig. 10. (a) Annual SoC Evolution for the BESS during the scheduling horizon. (b) Non-linear efficiency results obtained a posteriori from the optimisation.

4. Results

The results section presents the outcomes of two distinct schedulers. The first analysis validates the proposed advanced BESS model through an annual deterministic simulation. A simplified microgrid configuration, consisting of a single diesel generator, is used to clearly highlight the performance of the proposed BESS model. The results are compared against two benchmark models: one assuming constant efficiency without ageing and another assuming constant efficiency with calendar and cycle ageing. This comparison highlights the necessity of adopting a detailed BESS model to accurately represent the non-linear performance of the system. The first section closes with a sensitivity analysis on the calendar ageing coefficient used as input for the advanced BESS model.

The second analysis integrates the advanced BESS model into the chance-constrained optimisation framework and examines the impact of this formulation on microgrid operation. Lastly, a second sensitivity analysis on the spinning reserve confidence levels clarifies the role of the BESS in an isolated microgrid. All simulations were performed on a workstation equipped with an Intel Xeon W-2145 CPU (3.7 GHz) and 32 GB of RAM. The optimisation was implemented in Python and solved using Gurobi 13.0 with a MIP gap of 1%.

4.1. Advanced BESS model validation

The first section of the results validates the BESS model proposed in this paper. To highlight the accuracy of the model and its limited computational effort, we decided to run a simpler optimisation algorithm at this stage. The optimisation adopted for the validation assumes that the microgrid is operated with a single diesel genset that acts as a slack bus and does not have any binary variables. The scheduling horizon is one year with a sampling period of 1 h. This framework, thanks to the limited number of binary variables, ensures a fast convergence, but it still represents a good benchmark for the advanced BESS model since it has 8760 time instants to optimise and allows for the limited computational effort of the model developed.

The piecewise affine method adopted to represent the BESS non-

Table 5
Microgrid configuration tested.

Parameter	Value
PV nominal power [MWp]	10
BESS nominal power [MW]	5
BESS nominal energy [MWh]	10
Number of diesel generators	13
Single diesel generator apparent power [MVA]	2
Single diesel generator minimum power [MW]	1.4
Energy lost cost [€/kWh]	0.6
Diesel cost [€/kWh]	0.6
Cycle ageing coefficient (B)	1.332e^−5
τ [MW]	10

Table 6
Impact of the penalisation factor in the objective function.

Penalisation factor in the objective function	Relative value [%]
Charge losses ($Losses_t^{cha}$)	0.003664
Discharge losses ($Losses_t^{dis}$)	0.002969
Calendar ageing coefficient ($A(SoC)_t$)	0.001691

linear phenomena allows to perfectly interpolate the segments defined from the input values. Fig. 8a represents the charge and the discharge losses interpolation as a function of the BESS power. Fig. 8b depicts the interpolation of the calendar ageing coefficient as a function of the SoC. Both figures demonstrate the effectiveness of the linearisation method adopted in this work, since all operating points lie precisely on the interpolation segments.

The linearization of the calendar ageing coefficient dependency with the SoC allowed to properly represents the growth of SEI during the first year of BESS operation. Fig. 9a illustrates the impact that the piecewise affine formulation has on the calendar ageing trajectory in a day. When the SoC is higher than 50%, the contribution of the calendar ageing to the capacity fade increases following the trend specified in the case study. Fig. 9b represents the contribution of the cycle ageing at any specific time instant. The FEC rules the cycle ageing trend, and since a higher power linearly relates to the FEC, the cycle ageing contribution changes as a function of the BESS DC power. The cycle and the calendar ageing model implemented in the MILP enable the assessment of the system capacity fade. Fig. 9c represents the calendar and cycle ageing contribution computed inside the MILP problem for a year of operation.

Fig. 10a shows the SoC evolution of the BESS during the optimisation horizon. The figure highlights the capacity fade implemented within the optimisation framework. The capacity of the system reduces throughout the simulation as a function of the cycle and the calendar ageing computed inside the optimisation. Fig. 10b represents the efficiency of the system computed a posteriori with the processing of the interpolated charge and discharge losses from the MILP. The efficiency values obtained from the optimisation follow the benchmark efficiency (shadowed lines) of the BESS with a MAE of 1.03%.

Lastly, the piecewise affine interpolation requires a penalisation factor in the objective function to ensure that the interpolation values remain on the correct interpolation segments. Without this term, the solver could position values above the interpolating segment, which, although unlikely in cases involving losses or ageing minimisation, may occur when satisfying problem constraints requires deviating from physically consistent values. Therefore, a dedicated penalisation factor is included in the objective function for each interpolation, and their role in guaranteeing the correct behaviour of the piecewise affine interpolation is essential. To demonstrate that these penalisation factors have a negligible impact on the objective function, Table 5 represents the relative value of each penalisation factor against the overall value of the objective function. It is possible to observe that the maximum value of the penalisation factor is 0.0036%, which is lower than the MIP gap adopted and therefore could be considered negligible.

To highlight the importance of an advanced BESS model in microgrid scheduling, the solution proposed is compared with two models: A constant efficiency BESS model and a constant efficiency model that includes the capacity fade structure developed. The constant efficiency models use an efficiency value equal to 94% for both charge and discharge phases.

Table 6 summarises the structure of the models investigated and the results obtained in the validation procedure. The binary variables in all the models are related exclusively to the BESS charge and discharge dichotomy. Notably, the advanced model proposed does not use supplementary binary variables, and it is capable of effectively linearising efficiency and ageing with a limited computational effort. Since all models share the same number of binary variables, and as stated in [53] a MILP with a fixed number of integer variables is solvable in polynomial

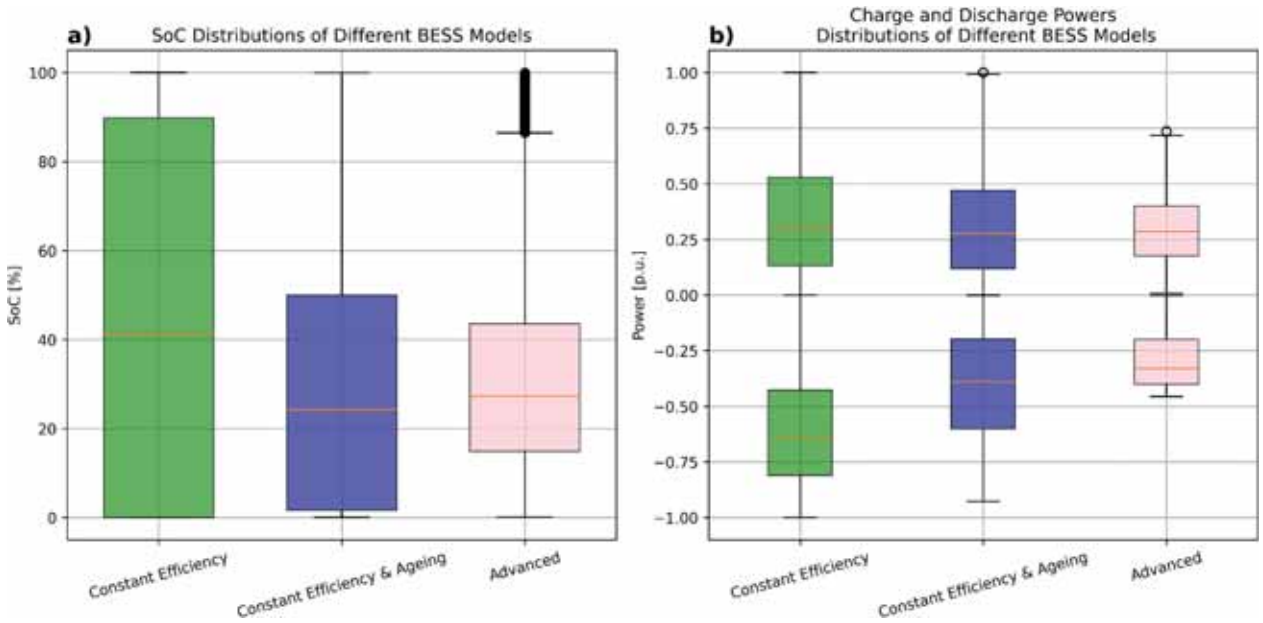

Fig. 11. Comparison of the SoC (a) and powers (b) distributions during a yearly simulation for the BESS model evaluated.

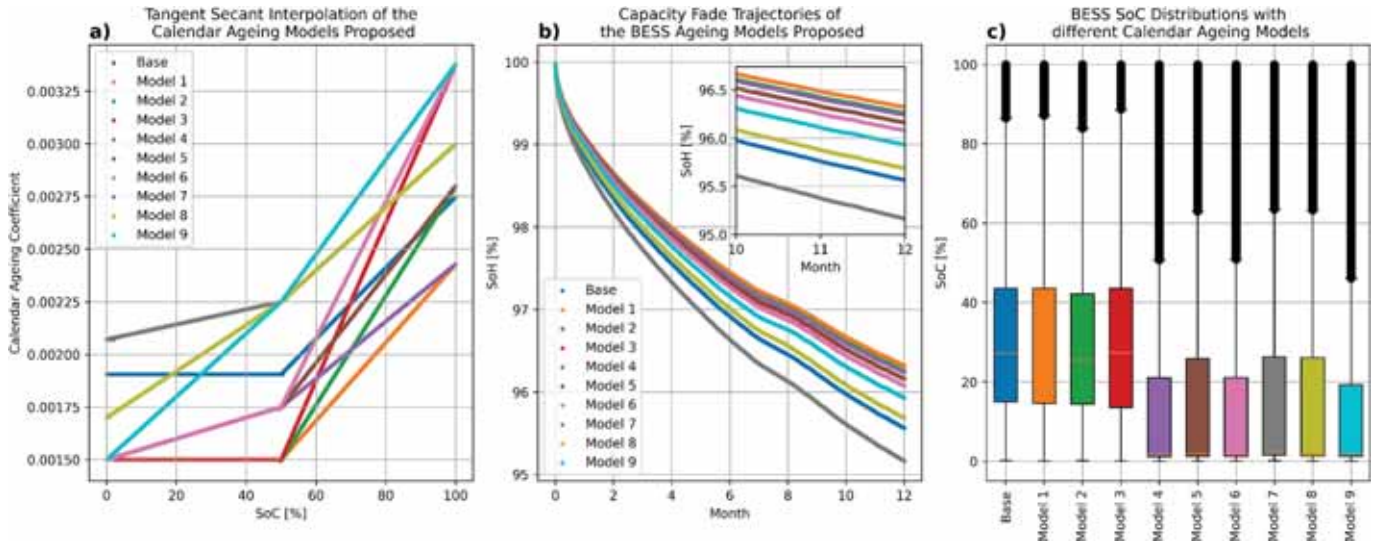

Fig. 12. Calendar ageing contributions computed by the optimisation for each model in the sensitivity analysis (a), corresponding capacity fade trajectories over a one-year simulation (b), and SoC distributions across the different model configurations (c).

Table 7
Parameters and results of the optimisation used to validate the proposed BESS model.

Parameter	No BESS	Constant efficiency model	Constant efficiency with ageing	Proposed BESS model
Binary variables	0	17,520	17,520	17,520
Constraints	35,040	122,642	192,722	315,362
Number of variables	35,040	236,522	262,802	280,322
MipGap [%]	0	0.0	0.896	0.05
Computational effort [s]	0.06	3.1	12.15	19.12
Objective function [€]	1,193,838	1,050,282	1,056,572	1,052,911
Savings generated by the BESS [€]	0	143,556 (+1.27%)	137,266 (−3.16%)	141,749
FEC	\	252.85 (+2.86%)	246.39 (+0.24%)	245.8
SoH [%]	\	100	95.51	95.56

Table 8
Technical and economic performances of the advanced BESS model with different calendar ageing coefficients.

Model	SoH [%]	MG cost [€]	BESS savings [€]	SoH relative [%]	MG cost relative [%]	BESS relative savings [%]
Base	95,56	1,052,911	140,927	0	0	0
Model 1	96,31	1,052,314	141,523	0,79	−0,05	0,42
Model 2	96,25	1,052,362	141,475	0,72	−0,05	0,38
Model 3	96,16	1,052,407	141,430	0,62	−0,04	0,35
Model 4	96,23	1,052,283	141,555	0,70	−0,05	0,44
Model 5	96,16	1,052,787	141,051	0,62	−0,01	0,08
Model 6	96,07	1,052,409	141,429	0,53	−0,04	0,35
Model 7	95,16	1,053,613	140,224	−0,41	0,06	−0,49
Model 8	95,68	1,053,574	140,263	0,12	0,06	−0,47
Model 9	95,92	1,052,519	141,318	0,38	−0,03	0,27

time with respect to the number of continuous variables and constraints, the computational complexity of the advanced model proposed remains consistent and scalable. The solver takes only 19.12 s to identify the BESS optimal schedule for a whole year for the advanced BESS model; this is a minor computational effort if compared to the very simple constant efficiency model (solved in 3.1 s). Furthermore, the MIP gap convergence criteria has been set to 1%, but a MIP gap of 0.0519% is reached. The computational efficiency of the proposed BESS formulation is further evidenced by the fact that the solver converged at the root node, without exploring any branch-and-cut nodes, indicating a tight linear relaxation and a strong MILP formulation [54]. From the comparison of the three models, it is possible to state that the constant-efficiency model exhibits lower computational effort and yields performance metrics comparable to those of the proposed formulation. However, it completely neglects the evolution of the state of health, resulting in significant limitations when applied to planning studies. The constant efficiency model with the capacity fade mechanisms enables a more accurate representation of battery degradation. However, the omission of variable efficiency introduces an error of up to 3.16% in the estimation of the cost savings generated by the BESS, leading to important approximation in the techno-economic analysis. Additionally, it should be noted that the objective function gap between the BESS models is three orders of magnitude larger than the penalisation factors adopted for the piecewise affine interpolation in the advanced model, further confirming that their impact on the optimisation is negligible.

Further clarification of the performance differences among the three models is provided in Fig. 11. Fig. 11a compares the SoC distributions of the three BESS models analysed in this section. The constant efficiency model, which does not include ageing constraints, allows the SoC to vary freely across the full operating range between 0 and 100%. In contrast, both the advanced model proposed in this work and the constant efficiency model with ageing constraints maintain the upper quartile of the SoC distribution below approximately 50%. This behaviour is mainly driven by calendar ageing considerations included in the two models. Calendar ageing has a significant impact on the capacity fade of cells, particularly during the first years of operation. For this reason, the optimisation strategy avoids prolonged operation at high SoC levels, reducing degradation and improving the expected lifetime of the storage asset. Fig. 11b compares the charge and discharge power distributions of the three models. The two models based on constant efficiency assumptions show relatively similar power distributions, with no

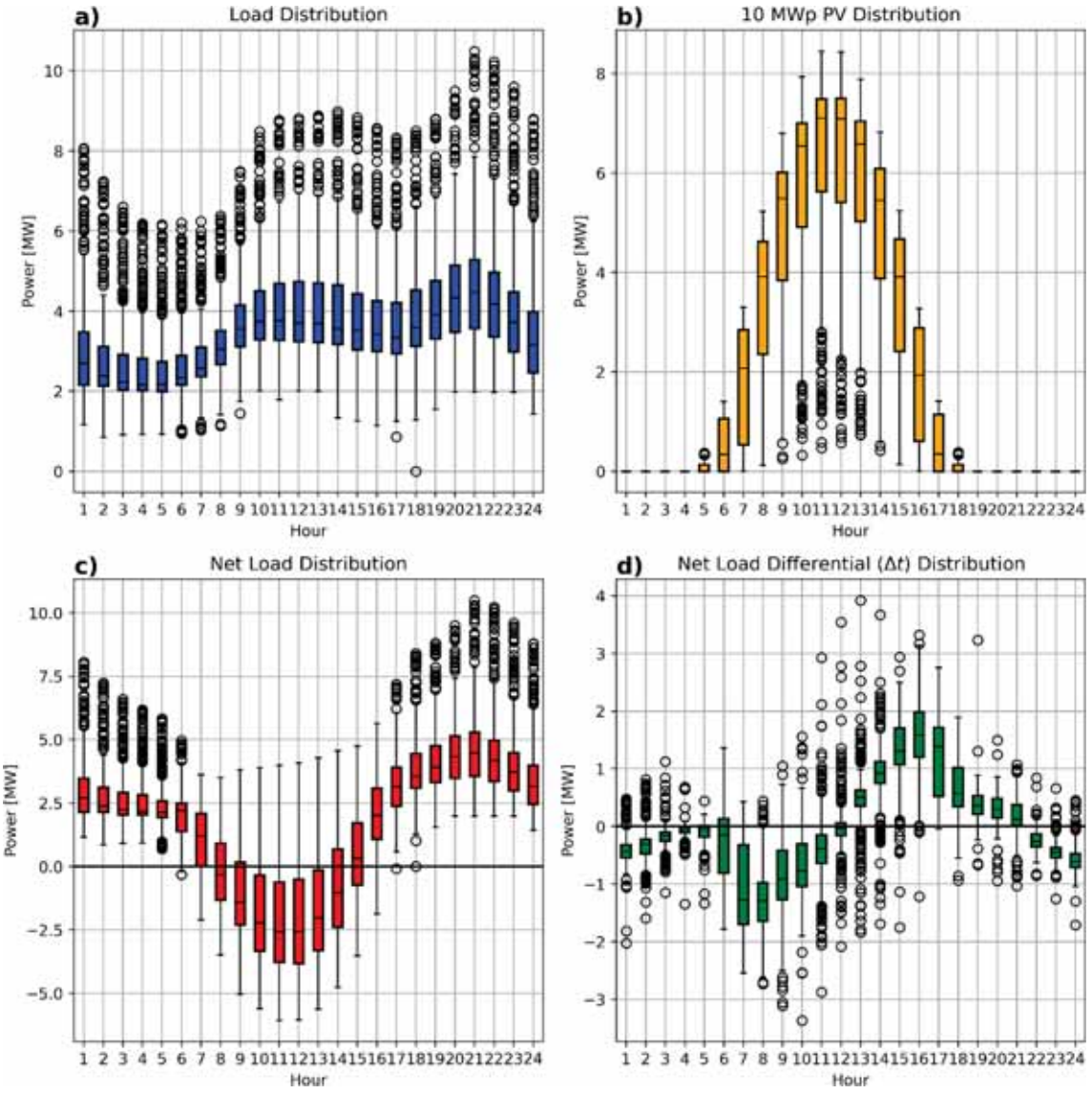

Fig. 13. Load (a), PV (b), net load (c), and net load differential (d) hourly probability power distribution.

significant differences in operating patterns. Conversely, the advanced model constrains both the charging and discharging power mainly within the 0.2–0.4 p.u. range, corresponding to the operating region where the BESS exhibits the highest efficiency. This demonstrates that including a more detailed representation of battery efficiency and ageing leads to optimisation toward better operating conditions that limit the degradation and preserve long-term asset performance.

4.1.1. Calendar ageing coefficients sensitivity analysis

The sensitivity analysis compares the advanced model validated in the previous section with the nine other BESS models that have different calendar ageing coefficients presented in Table 3. The scope of the sensitivity analysis is to assess the robustness of the piecewise affine interpolation with different coefficients and the role that calendar ageing has on the BESS capacity fade and on the objective function.

The results reported in Fig. 12a show the calendar ageing contribution computed by the optimisation as a function of SoC for all models included in the sensitivity analysis over a yearly simulation. The piecewise affine interpolation correctly operates for all the models proposed. Fig. 12b details the capacity-fade (calendar + cycle) trajectories obtained with the different calendar ageing coefficients for a yearly simulation. Model 1 and Model 7 are the upper and lower boundaries of the capacity fade trajectories computed by the advanced BESS model. The capacity fade difference between the two models is 1.15%. Fig. 12c reports the SoC distribution of the BESS with different calendar ageing segments. Notably, the coefficients selected for Model 9 have the greatest angular coefficient for both 0% to 50% and to 50% to 100%. This could translate into a high capacity fade due to calendar ageing, but the results show that Model 9 has the fourth-worst capacity fade. The advanced BESS model acknowledges the risk elevate capacity fade that the BESS could experience due to high SoC and strongly limits the system operation in the upper SoC region, reducing the degradation of the asset.

Table 7 summarises the technical and economic results of the sensitivity analysis on the calendar ageing coefficients of the advanced BESS model, with the base case acting as the reference for all related metrics. Despite capacity fade variations of up to 0.7% from the benchmark, the influence on microgrid cost proves practically negligible, with a maximum deviation of 0.06%. An equivalent conclusion applies to the BESS savings, where the maximum deviation from the benchmark stands at −0.49% from Model 9. Therefore, uncertainty in the calendar-ageing coefficients mainly affects the capacity fade of the BESS and its operation. Although, as demonstrated in the previous paragraph, the inclusion of the calendar ageing is essential, the

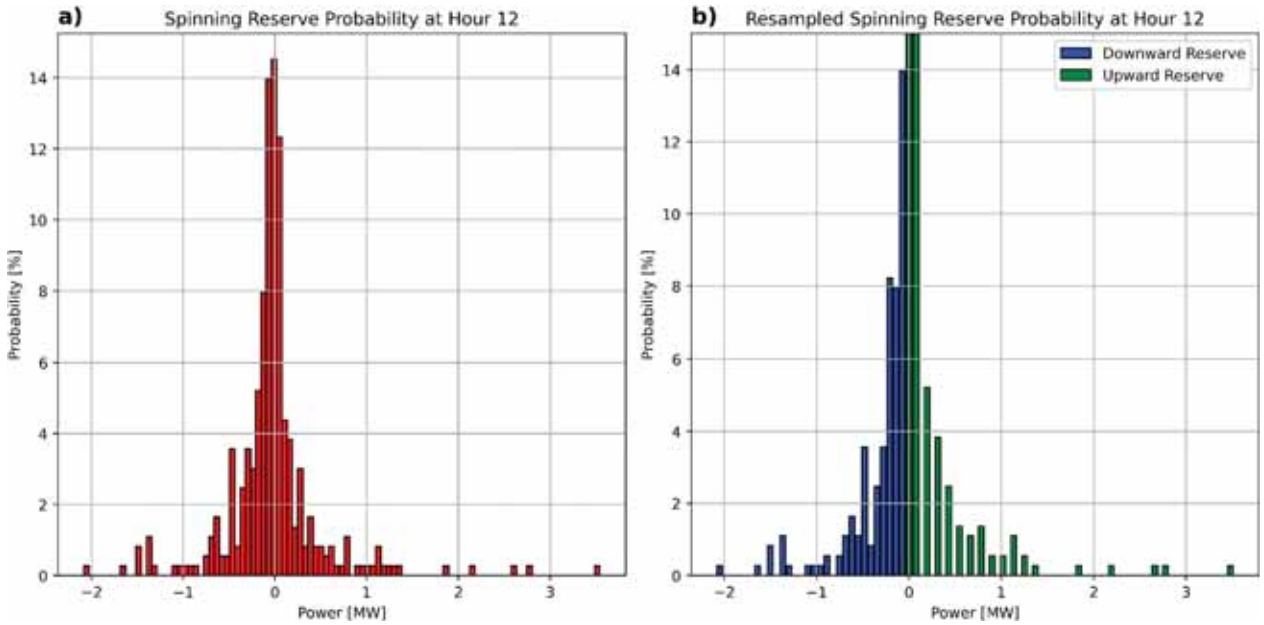

Fig. 14. Spinning reserve probability (a) and consequent discrete upward and downward spinning reserve (b) used as input for the chance-constrained scheduling problem.

uncertainty of the parameters adopted has a limited impact on the overall microgrid economics (Table 8).

4.2. Chance constrained microgrid scheduling

The procedure developed processes the PV and load profiles and generates a set of discrete probability functions of upward and downward spinning reserve used as input for the chance constrained optimisation. Given the load and PV data distribution, respectively depicted in Fig. 13a and b, the net load distribution, shown in Fig. 13c is obtained as the difference between load consumption and PV production at each time instant. The net load differential distributions (in green) are then used to generate the discrete probability density functions that define the spinning reserve requirements. Fig. 13d illustrates the outcome of the methodology applied to determine the net load differential used in constructing the spinning reserve probability density function.

The net load differential distribution requires further processing to be applied within the MILP. Specifically, the positive and negative values of the net load distribution are decoupled into upward and downward reserves. Both upward and downward reserves are discretised into 30 intervals as suggested in [55]. Fig. 14 illustrates the outcome of the discretisation procedure. Fig. 14a shows the probability density function of the first hour of the day for the net load differential. Fig. 14b depicts the outcome of the conversion procedure that takes the initial function and generates two discrete probability density functions with 30 intervals each, suitable for the MILP formulation. The procedure defines several magnitudes of spinning reserve and their probability of occurrence. These two parameters, reserve magnitude and probability of occurrence, are determined for every hour and serve as key inputs to the chance-constrained MILP model.

The MILP model uses as input parameters the PV production, load consumption of the selected day, and the discrete probability function of the spinning reserves to determine the microgrid's optimal schedule. Fig. 15 illustrates an example of the decision variables selected by the MILP with a spinning reserve confidence level (α) equal to 0.5. Fig. 15a represents the consumption side of the system. Here, the energy balance equality constraints allow the advanced BESS model either to charge the BESS with surplus energy or, in cases of significant overproduction, to curtail excess generation. Fig. 15b depicts the production side of the system. Since there is no intrinsic advantage in discharging the BESS at a specific moment, the timing of discharge is determined primarily by the spinning reserve requirements. Fig. 15c shows the evolution of the BESS variables during optimisation, where the state of charge changes between 0% and 100%, indicating full utilisation of the storage capacity. Finally, Fig. 15d presents the spinning reserve requirement of the microgrid, defined according to the specified confidence level α. Notably, the results show that the BESS supplies almost the entirety of the spinning reserve. This outcome is driven by the fact that BESS-based reserve provision incurs no additional cost, whereas reserve provision from diesel generators often requires start-up or activation of additional units, thereby increasing operational costs. Therefore, the installation of a BESS in the microgrid reduces the operational cost of the spinning reserve.

The solver required 1.31 s to optimise 24 time steps with 1921 binary variables, achieving a final MIP gap of 0.8391%. These results prove the reliability and the low computational effort of the modelling solution adopted.

4.3. Sensitivity analysis on the chance-constrained formulation

This section analyses the impact of relevant input parameters on the optimisation outcomes. First, the influence of the selected confidence level on the chance-constrained spinning reserve formulation is examined. The analysis is then extended to different BESS sizes to clarify the relationship between microgrid reliability, costs, storage nominal power and nominal energy. Lastly, we show the interpolating performances of the piecewise affine interpolation, demonstrating its robustness in all the scenarios tested.

The confidence level α selected as an input is strictly correlated to the quantity of spinning reserve that the system must ensure. Fig. 16 shows the hourly microgrid spinning reserve scheduled by MILP with different values of confidence level. The figure highlights how the confidence level α influences the spinning reserve requirement. A confidence level of $\alpha = 1$ implies that the microgrid must satisfy all possible realisations of the spinning reserve at every optimisation step. In other words, the optimisation fully covers the spinning reserve values obtained from the discrete probability distribution. Reducing the confidence level relaxes this requirement, allowing the microgrid to be less constrained in

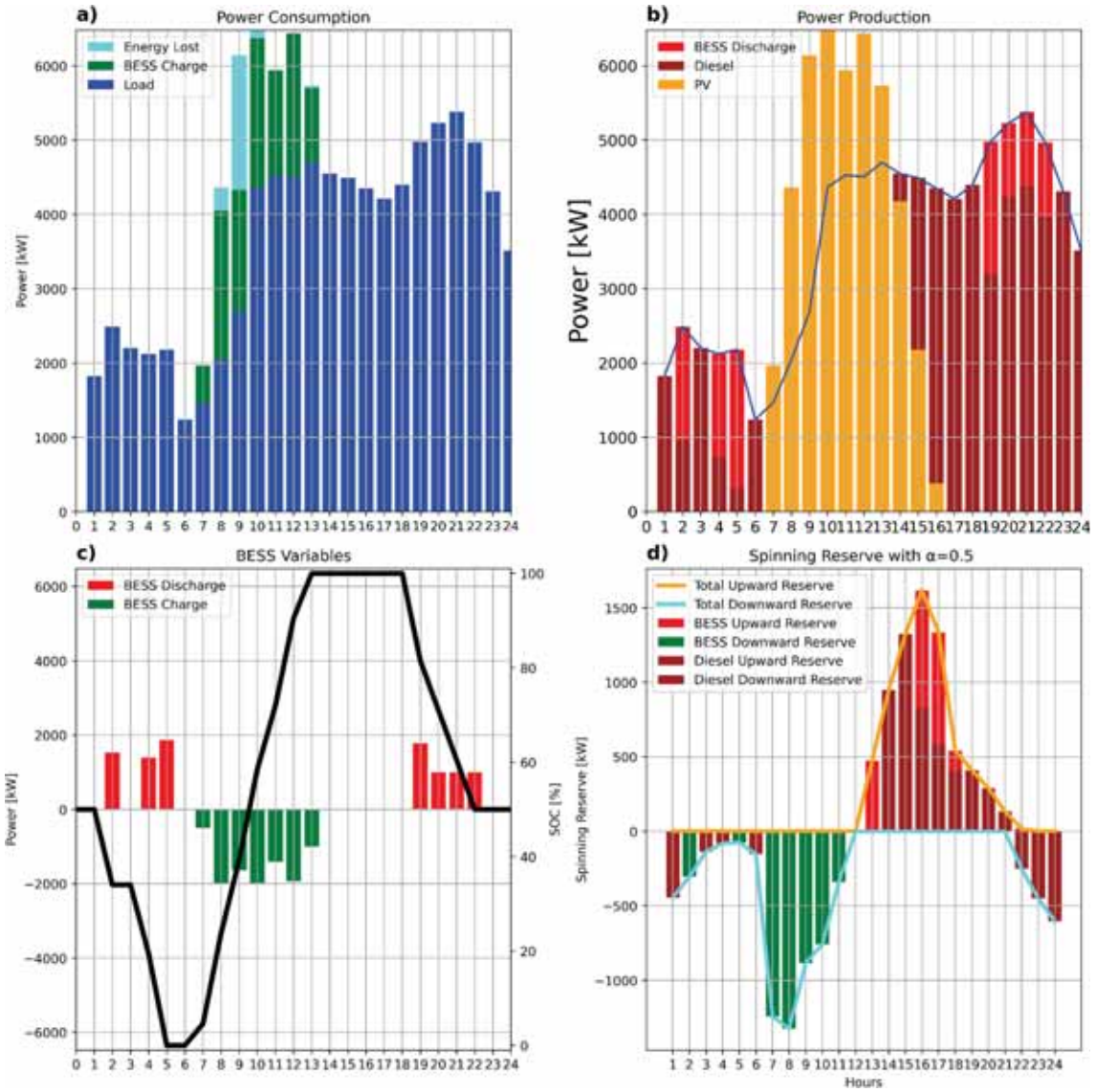

Fig. 15. Outcome of the chance constrained MILP decision variables for a typical day of the optimisation problem.

providing spinning reserve.

A comparison between microgrid costs at different confidence levels highlights the influence of the chance-constrained approach on the optimisation outcomes. Fig. 17a represents the relative microgrid cost ($R_{Microgrid}$) variation as a function of the optimisation confidence level, the BESS nominal power, and the energy-to-power ratio.

In the absence of a BESS, the spinning reserve is entirely provided by diesel generators. As the confidence level increases, a larger amount of spinning reserve is required, which forces additional generators to remain active, thereby raising microgrid costs. The coverage of all the possible realisations of the spinning reserve requires an increase in the cost equal to 78%.

Installing a BESS enable the provision of spinning reserve at no additional operating cost. As a consequence, the operating costs of the microgrid decrease because storage assets can fully or partially cover the spinning reserve requirements without additional fuel or start-up costs. It is particularly important to note that both the power and energy ratings of the BESS significantly affect the microgrid's relative cost. This outcome is consistent with the problem constraints. The spinning reserve contribution of the BESS depends on its nominal energy and power. Since this spinning reserve from the BESS is effectively "free," the optimisation maximises its use. As a result, if the BESS nominal power and the current SoC are sufficient to cover the reserve requirements, variations in the confidence level no longer impact microgrid costs. The analysis allows to state that the presence of a BESS in an isolated microgrid ensures the achievement of higher levels of reliability without increasing the operating costs of the system. The largest BESS configuration tested reach the 100% of reliability with an increase in the operating cost equal to 4.29%.

Lastly, Fig. 17b depicts the interpolation accuracy of the piecewise affine method for BESS losses across all BESS sizes evaluated in the sensitivity analysis. For every configuration, the operating points identified by the optimisation closely align with the reference losses function, confirming the robustness of the approach across a wide range of rated powers and energies.

5. Conclusions, limitations & future works

This paper presented an advanced battery energy storage system (BESS) model for the scheduling of isolated microgrids under uncertainty, incorporating a chance-constrained formulation for spinning reserve requirements. The proposed BESS model accurately represents both efficiency variations and battery ageing through a computationally efficient linearised formulation. The resulting optimisation framework

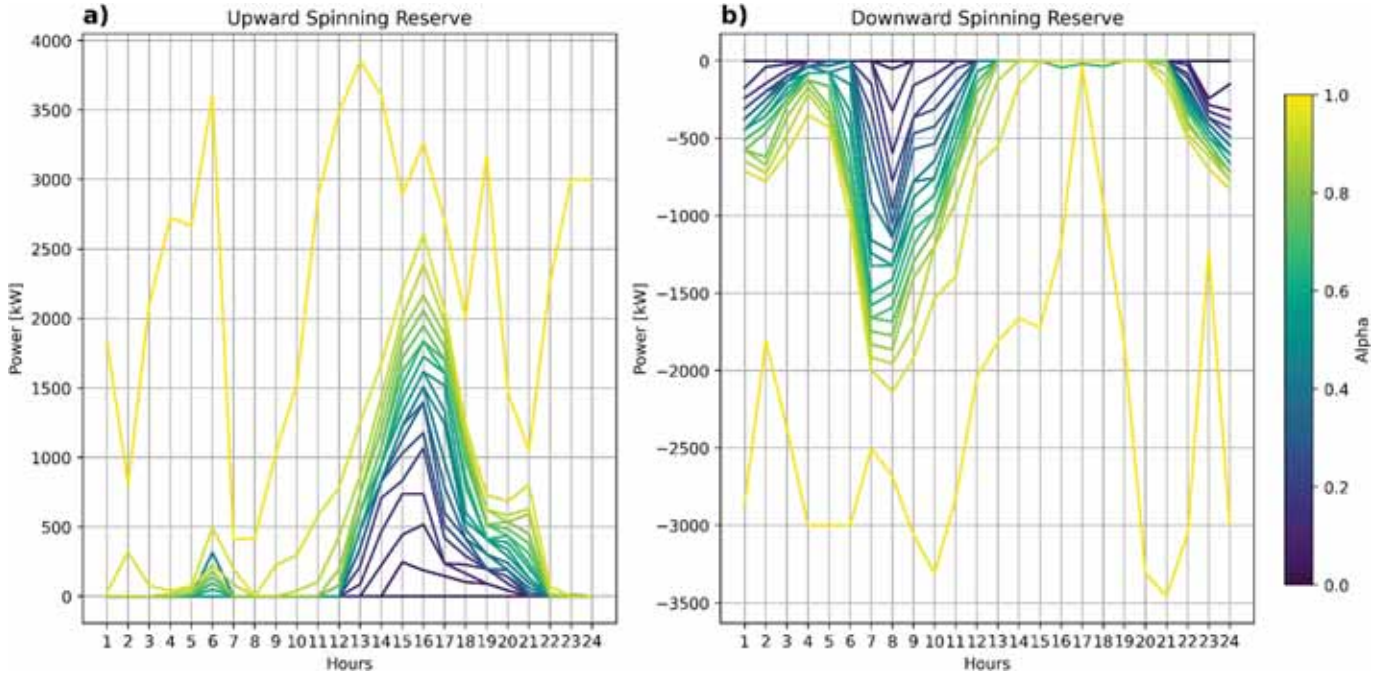

Fig. 16. Variation of the upward and downward spinning reserve as a function of the confidence level alpha.

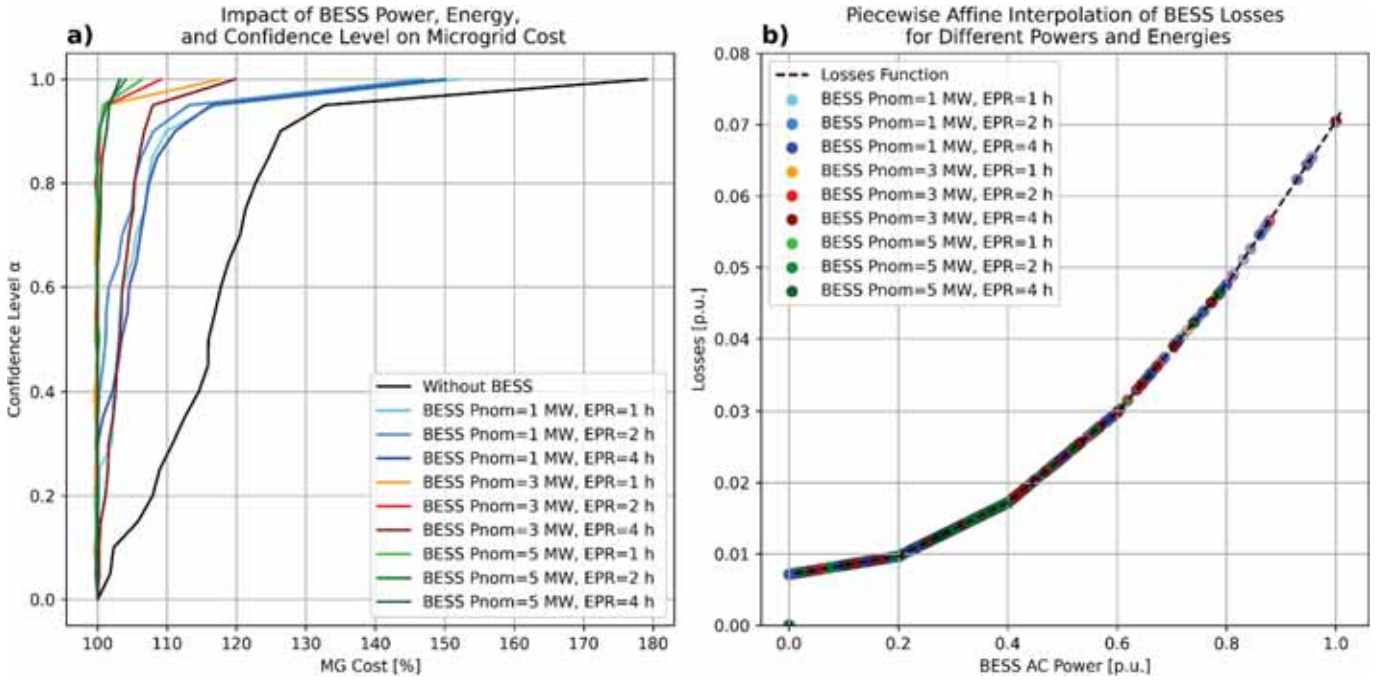

Fig. 17. Relationship between the relative microgrid cost and the optimisation parameters (a) and performance of the piecewise affine interpolation of the losses in the scenarios evaluated.

enables the scheduling of a full year of operation in less than 20 s while achieving a MAE of 1.03% with respect to a detailed efficiency reference model. These features make the proposed approach well-suited not only for operational studies but also for long-term planning applications. The inclusion of ageing and efficiency in the optimisation framework is fundamental since the absence of one of these characteristics may lead to an error of up to 3% in the savings generated by the BESS. Furthermore, the sensitivity analysis on the calendar ageing coefficients showed that, although uncertainty in calendar ageing significantly affects the long-term capacity fade of the BESS, its impact on the overall microgrid economics remains negligible.

The inclusion of chance-constrained optimisation in the methodology has a twofold objective. Firstly, it allows for modelling the uncertainty in the spinning reserve requirements with negligible additional computational burden. Secondly, it tests the correct working of the advanced BESS model developed. The sensitivity analysis demonstrates that the integration of BESS significantly enhances microgrid reliability while limiting operating costs, highlighting the critical role of storage systems in isolated microgrids with high renewable penetration.

Future work will focus on extending the proposed framework to

address additional services provided by BESS in isolated microgrids, such as inertia support and primary frequency containment, which are not explicitly considered in the current formulation. The analysis will compare the outcome of the optimisation with the dynamic model of the microgrid to understand the advantages and the limits of the formulations proposed.

CRediT authorship contribution statement

Matteo Spiller: Writing – original draft, Validation, Methodology, Formal analysis, Conceptualization. **Riccardo Nebuloni:** Conceptualization. **Marco Merlo:** Writing – review & editing, Validation, Supervision, Conceptualization.

Declaration of competing interest

The authors declare that they have no known competing financial interests or personal relationships that could have appeared to influence the work reported in this paper.

Acknowledgments

The authors would like to thank *Società Elettrica Liparese* for providing the data and for their valuable support in the development of the case study.

Data availability

Data will be made available on request.

References

[1] A. Shivakumar, A. Dobbins, U. Fahl, A. Singh, Drivers of renewable energy deployment in the EU: an analysis of past trends and projections, Energ. Strat. Rev. 26 (Nov. 2019) 100402, https://doi.org/10.1016/J.ESR.2019.100402.
[2] M.H. Saeed, W. Fangzong, B.A. Kalwar, S. Iqbal, A review on microgrids' challenges perspectives, IEEE Access 9 (2021) 166502–166517, https://doi.org/10.1109/ACCESS.2021.3135083.
[3] IEA, Batteries and secure energy transitions, Available: https://www.iea.org/reports/batteries-and-secure-energy-transitions, 2024. (Accessed 22 December 2025) (Online).
[4] L.T. Dos Santos, M. Sechilariu, F. Locment, Day-ahead microgrid optimal self-scheduling: comparison between three methods applied to isolated DC microgrid, in: IECON Proceedings (Industrial Electronics Conference), Feb. 2014, pp. 2010–2016, https://doi.org/10.1109/IECON.2014.7048778.
[5] H. Morais, P. Kádár, P. Faria, Z.A. Vale, H.M. Khodr, Optimal scheduling of a renewable micro-grid in an isolated load area using mixed-integer linear programming, Renew. Energy 35 (1) (Jan. 2010) 151–156, https://doi.org/10.1016/J.RENENE.2009.02.031.
[6] D.K.Y. Rebours, What Is Spinning Reserve?, Sep. 2005.
[7] M.A. Ortega-Vazquez, D.S. Kirschen, Optimizing the spinning reserve requirements using a cost/benefit analysis, IEEE Trans. Power Syst. 22 (1) (Feb. 2007) 24–33, https://doi.org/10.1109/TPWRS.2006.888951.
[8] M.A. Ortega-Vazquez, D.S. Kirschen, Should the spinning reserve procurement in systems with wind power generation be deterministic or probabilistic?, in: 1st International Conference on Sustainable Power Generation and Supply, SUPERGEN '09, 2009, https://doi.org/10.1109/SUPERGEN.2009.5348164.
[9] H.B. Gooi, Optimal scheduling of spinning reserve, IEEE Trans. Power Syst. 14 (4) (1999) 1485–1492, https://doi.org/10.1109/59.801936.
[10] M.Q. Wang, H.B. Gooi, Spinning reserve estimation in microgrids, IEEE Trans. Power Syst. 26 (3) (Aug. 2011) 1164–1174, https://doi.org/10.1109/TPWRS.2010.2100414.
[11] Y.Y.Z.Z.D. Li, Optimal scheduling of an isolated microgrid with battery storage considering load and renewable generation uncertainties, Available: https://www.researchgate.net/publication/343053809_Optimal_Scheduling_of_an_Isolated_Microgrid_with_Battery_Storage_Considering_Load_and_Renewable_Generation_Uncertainties, 2018. (Accessed 28 August 2025).
[12] Y.G. Park, C.W. Kim, J.B. Park, MILP-based dynamic efficiency scheduling model of battery energy storage systems, J. Electr. Eng. Technol. 11 (5) (Sep. 2016) 1063–1069, https://doi.org/10.5370/JEET.2016.11.5.1063.
[13] H. Pandžić, V. Bobanac, An accurate charging model of battery energy storage, IEEE Trans. Power Syst. 34 (2) (Mar. 2019) 1416–1426, https://doi.org/10.1109/TPWRS.2018.2876466.
[14] C. Zhao, P.B. Andersen, C. Træholt, S. Hashemi, Grid-connected battery energy storage system: a review on application and integration, Renew. Sust. Energ. Rev. 182 (Aug. 2023) 113400, https://doi.org/10.1016/J.RSER.2023.113400.
[15] R. Nebuloni, et al., A hierarchical two-level MILP optimization model for the management of grid-connected BESS considering accurate physical model, Appl. Energy 334 (Mar. 2023) 120697, https://doi.org/10.1016/J.APENERGY.2023.120697.
[16] F. Bovera, M. Spiller, M. Zatti, G. Rancilio, M. Merlo, Development, validation, and testing of advanced mathematical models for the optimization of BESS operation, Sustain. Energy Grids Netw. 36 (Dec. 2023) 101152, https://doi.org/10.1016/J.SEGAN.2023.101152.
[17] A. Vasylyev, A. Vannoni, A. Sorce, Optimal dispatch of Li-ion battery energy storage, reviewing and considering cycling and calendar ageing models, Appl. Therm. Eng. 265 (Apr. 2025) 125597, https://doi.org/10.1016/J.APPLTHERMALENG.2025.125597.
[18] M. Pakjoo, et al., A review on testing of electrochemical cells for aging models in BESS, Energies 16 (Sep. 2023) 6887, https://doi.org/10.3390/EN16196887.
[19] S.S. Madani, et al., A comprehensive review on lithium-ion battery lifetime prediction and aging mechanism analysis, Batteries 11 (4) (Mar. 2025) 127, https://doi.org/10.3390/BATTERIES11040127.
[20] G. He, Q. Chen, C. Kang, P. Pinson, Q. Xia, Optimal bidding strategy of battery storage in power markets considering performance-based regulation and battery cycle life, IEEE Trans. Smart Grid 7 (5) (Sep. 2016) 2359–2367, https://doi.org/10.1109/TSG.2015.2424314.
[21] C. Liu, H. Ma, H. Zhang, X. Shi, F. Shi, A MILP-based battery degradation model for economic scheduling of power system, IEEE Trans. Sustain. Energy 14 (2) (Apr. 2023) 1000–1009, https://doi.org/10.1109/TSTE.2022.3232370.
[22] R. Nebuloni, et al., A MILP battery degradation logarithmic model with real-time cycle counting calculation, IEEE Trans. Ind. Appl. 61 (6) (2025) 8297–8306, https://doi.org/10.1109/TIA.2025.3571359.
[23] M. Petrelli, D. Fioriti, A. Berizzi, D. Poli, Multi-year planning of a rural microgrid considering storage degradation, IEEE Trans. Power Syst. 36 (2) (Mar. 2021) 1459–1469, https://doi.org/10.1109/TPWRS.2020.3020219.
[24] T.M. Masaud, E. El-Saadany, Optimal battery planning for microgrid applications considering battery swapping and evolution of the SOH during lifecycle aging, IEEE Syst. J. 17 (3) (Sep. 2023) 4725–4736, https://doi.org/10.1109/JSYST.2023.3285147.
[25] M.M. Hasan, et al., Advancing energy storage: the future trajectory of lithium-ion battery technologies, J. Energy Storage 120 (Jun. 2025) 116511, https://doi.org/10.1016/J.EST.2025.116511.
[26] Y. Preger, et al., Degradation of commercial lithium-ion cells as a function of chemistry and cycling conditions, J. Electrochem. Soc. 167 (12) (Jan. 2020) 120532, https://doi.org/10.1149/1945-7111/ABAE37.
[27] S. Barcellona, L. Piegari, Effect of current on cycle aging of lithium ion batteries, J. Energy Storage 29 (Jun. 2020) 101310, https://doi.org/10.1016/J.EST.2020.101310.
[28] G. Saldaña, J.I.S. Martín, I. Zamora, F.J. Asensio, O. Oñederra, M. González-Pérez, Empirical calendar ageing model for electric vehicles and energy storage systems batteries, J. Energy Storage 55 (Nov. 2022) 105676, https://doi.org/10.1016/J.EST.2022.105676.
[29] E. Redondo-Iglesias, P. Venet, S. Pelissier, Eyring acceleration model for predicting calendar ageing of lithium-ion batteries, J. Energy Storage 13 (Oct. 2017) 176–183, https://doi.org/10.1016/J.EST.2017.06.009.
[30] R. Khezri, D. Steen, E. Wikner, L.A. Tuan, Optimal V2G scheduling of an EV with calendar and cycle aging of battery: an MILP approach, IEEE Trans. Transp. Electrification 10 (4) (2024) 10497–10507, https://doi.org/10.1109/TTE.2024.3384293.
[31] M. Amini, M.H. Nazari, S.H. Hosseinian, Predictive energy management strategy for battery energy storage considering battery degradation cost, IET. Renew. Power Gener. 17 (5) (Apr. 2023) 1119–1138, https://doi.org/10.1049/RPG2.12669. PAGE:STRING:ARTICLE/CHAPTER.
[32] G. Liu, M. Starke, B. Xiao, K. Tomsovic, Robust optimisation-based microgrid scheduling with islanding constraints, IET Gener. Transm. Distrib. 11 (7) (May 2017) 1820–1828, https://doi.org/10.1049/IET-GTD.2016.1699.
[33] A. Sakti, et al., Enhanced representations of lithium-ion batteries in power systems models and their effect on the valuation of energy arbitrage applications, J. Power Sources 342 (Feb. 2017) 279–291, https://doi.org/10.1016/J.JPOWSOUR.2016.12.063.
[34] S.F. Schuster, et al., Nonlinear aging characteristics of lithium-ion cells under different operational conditions, J. Energy Storage 1 (1) (Jun. 2015) 44–53, https://doi.org/10.1016/J.EST.2015.05.003.
[35] J. Wang, et al., Degradation of lithium ion batteries employing graphite negatives and nickel–cobalt–manganese oxide + spinel manganese oxide positives: part 1, aging mechanisms and life estimation, J. Power Sources 269 (Dec. 2014) 937–948, https://doi.org/10.1016/J.JPOWSOUR.2014.07.030.
[36] K. Bischof, et al., Calendar aging of Lithium-Ion batteries, J. Electrochem. Soc. 163 (9) (Jul. 2016) A1872, https://doi.org/10.1149/2.0411609JES.
[37] J. Schmalstieg, K. Stefan, M. Ecker, D.U. Sauer, From Accelerated Aging Tests to a Lifetime Prediction Model: Analyzing Lithium-ion Batteries, 2013.
[38] G. Rancilio, et al., Modeling a large-scale battery energy storage system for power grid application analysis, Energies (Basel) 12 (17) (Aug. 2019), https://doi.org/10.3390/en12173312.
[39] Johannes Bisschop, AIMMS - Optimization Modelling, 2023.
[40] Terna, Esiti Asta MACSE anno di consegna 2028, Available: https://www.terna.it/en/electric-system/publications/operators-news/detail/pubblicazione-esiti-asta-macse-anno-consegna-2028, 2025. (Accessed 11 December 2025) (Online).
[41] H. Gan, J. Tian, H. Qiu, G. Li, C. Liu, J. Zhao, Thermal performance of symmetrical double-spiral channel liquid cooling plate based battery thermal management for

energy storage system, Appl. Therm. Eng. 263 (Mar. 2025) 125399, https://doi.org/10.1016/J.APPLTHERMALENG.2024.125399.
[42] V.N. Lam, X. Cui, F. Stroebl, M. Uppaluri, S. Onori, W.C. Chueh, A decade of insights: delving into calendar aging trends and implications, Joule 9 (1) (Jan. 2025) 101796, https://doi.org/10.1016/J.JOULE.2024.11.013.
[43] Battery archive, Available: www.batteryarchive.org, 2024. (Accessed 11 December 2025) (Online).
[44] K. Liu, T.R. Ashwin, X. Hu, M. Lucu, W.D. Widanage, An evaluation study of different modelling techniques for calendar ageing prediction of lithium-ion batteries, Renew. Sust. Energ. Rev. 131 (Oct. 2020) 110017, https://doi.org/10.1016/J.RSER.2020.110017.
[45] M. Spiller, et al., A model-aware comprehensive tool for battery energy storage system sizing, Energies 16 (18) (Sep. 2023) 6546, https://doi.org/10.3390/EN16186546.
[46] E. Redondo-iglesias, P. Venet, S. Pelissier, Calendar and cycling ageing combination of batteries in electric vehicles, Microelectron. Reliab. (October) (2018).
[47] M.S. Hosen, J. Jaguemont, J. Van Mierlo, M. Berecibar, Battery lifetime prediction and performance assessment of different modeling approaches, iScience 24 (2) (Feb. 2021) 102060, https://doi.org/10.1016/J.ISCI.2021.102060.
[48] J. Schmalstieg, S. Käbitz, M. Ecker, D.U. Sauer, A holistic aging model for Li (NiMnCo)O2 based 18650 lithium-ion batteries, J. Power Sources 257 (Jul. 2014) 325–334, https://doi.org/10.1016/J.JPOWSOUR.2014.02.012.
[49] D. Andreotti, M. Spiller, A. Scrocca, F. Bovera, G. Rancilio, Modeling and analysis of BESS operations in electricity markets: prediction and strategies for day-ahead and continuous intra-day markets, Sustainability 16 (18) (Sep. 2024), https://doi.org/10.3390/SU16187940.
[50] Z. Wang, S. Bu, J. Wen, C. Huang, A comprehensive review on uncertainty modeling methods in modern power systems, Int. J. Electr. Power Energy Syst. 166 (May 2025) 110534, https://doi.org/10.1016/J.IJEPES.2025.110534.
[51] A. Zakariazadeh, S. Jadid, P. Siano, Smart microgrid energy and reserve scheduling with demand response using stochastic optimization, Int. J. Electr. Power Energy Syst. 63 (Dec. 2014) 523–533, https://doi.org/10.1016/J.IJEPES.2014.06.037.
[52] Renewable Ninja. https://www.renewables.ninja/, 2016.
[53] M. Conforti, G. Cornuéjols, G. Zambelli, Integer Programming vol. 271, 2014, https://doi.org/10.1007/978-3-319-11008-0.
[54] J.P. Vielma, Mixed integer linear programming formulation techniques, SIAM Rev. 57 (1) (Feb. 2015) 3–57, https://doi.org/10.1137/130915303.
[55] B.K. Pagnoncelli, S. Ahmed, A. Shapiro, Sample average approximation method for chance constrained programming: theory and applications, J. Optim. Theory Appl. 142 (2) (Mar. 2009) 399–416, https://doi.org/10.1007/S10957-009-9523-6.